JPRS-CST-94-001
24 January 1994

JPRS Report

Science & Technology

China

Science & Technology
China

JPRS-CST-94-001 24 January 1994

CONTENTS

Computers

Lasers, Sensors, Optics

Microelectronics

Superconductivity

Telecommunications R&D

China, Japan Sign MOU on Receiving JERS-1 Data

94P60088B Beijing ZHONGGUO KEXUE BAO [CHINESE SCIENCE NEWS] in Chinese 20 Dec 93 p 1

[Article by Qiu Huasheng [6726 5478 4141]: "China, Japan Sign Memorandum on Receiving Japan Earth Resources Satellite Data"]

[Summary] CAS Vice President Yan Yixun [0917 5030 1053] and Japan's NASDA Director Masato Yamano recently signed in Tokyo a bilateral "Memorandum of Understanding on Direct Receiving and Distribution of Data From Japan's JERS-1 Earth Resources Satellite." State Councillor Song Jian and Japan's Science and Technology Agency Director-General Satsuki Eda attended the signing ceremony. According to the MOU, Japan will transmit data gathered by JERS-1 to the CAS Remote Sensing Satellite Ground Station without charge.

Software State Engineering Research Center Set for Shenyang

94P60088A Beijing KEJI RIBAO [SCIENCE AND TECHNOLOGY DAILY] in Chinese 18 Dec 93 p 1

[Article by Li Beidou [2621 0554 2435]: "Computer Software State Engineering Research Center Set for Shenyang"]

[Summary] The location of the nation's first state-level computer software engineering research center was officially set for Shenyang a few days ago. This new SERC, which will engage in computer multimedia software research, development, and commercialization, will grow out of the Northeast University Software Center, which reached a software production scale of 30 million yuan in 1993.

Tetradymite Discovery Made in Sichuan

94P60072A Chengdu SICHUAN RIBAO in Chinese 25 Oct 93 p 1

[Text] A tetradymite deposit has been discovered on the banks of the Dadu River in Shimian County, Sichuan Province. Rarely found, the tetradymite is regarded as a "national treasure."

Tellurium, a dispersed element, is an extremely important industrial raw material having broad application in metallurgy, the chemical industry, electronics, refrigeration, computers, pharmaceuticals, and national defense. Today, there are some 250 tons of tellurium produced in the whole world each year; China produces a mere 2 tons. The Sichuan Provincial Science Committee has placed the research and development of tellurium and bismuth on the agenda of major provincial scientific projects in 1993. Experts from the Ministry of Geology and Mineral Resources were directed to the Shimian site by the State Science and Technology Commission to investigate the situation. They firmly believe that this deposit not only constitutes an independent ore body, it also has industrial value. The Sichuan Nonferrous Rare and Precious Metals Company has established the Chengdu Xianjin Tellurium Company and Research Institute in Chengdu to study and develop rare dispersed elements and the separation of bismuth and tellurium. They are now pursuing an economic as well as advanced technology to separate bismuth and tellurium. Some initial results have been forthcoming: grades as high as 99.99 percent purity have been obtained. The next step will be to build a separation plant at Shimian to obtain precise scientific data.

Super-Resolution Imaging Diagnosis of Scattering Centers on Vehicle

40100027A Beijing YUHANG XUEBAO [JOURNAL OF ASTRONAUTICS] in Chinese
Vol 14 No 4, Oct 93 pp 1-7

[English abstract of article by Xu Xiaojian of the Beijing Institute of Environmental Features, the Second Academy, Ministry of Aero-Space Industry and Huang Peikang of the Science & Technology Committee of the Second Academy, Ministry of Aero-Space Industry; MS received 10 Sep 92]

[Text] High/super-resolution microwave diagnostic imaging of scattering centers is an important tool for the design of stealth vehicles. In the paper, the techniques of super-resolution imaging diagnosis are considered. Four imaging algorithms—the two-dimensional Fourier transform (2-D FFT) algorithm, the filtered back-projection algorithm (FBP), the maximum entropy spectral estimation (MESE) approach, and the artificial neural network (ANN) hybrid algorithm, are discussed. The four algorithms are used to reconstruct target images, and experimental results of imaging a model aircraft measured in an anechoic chamber are given.

Subject terms: Microwave Imaging, Electromagnetic Scattering, Vehicle, Stealth Technology, Radar Target

References

1. Huang Peikang et al., "Microwave Imaging of Targets Rotating in Small Azimuth Angle Range" [in Chinese], DIANZI XUEBAO [ACTA ELECTRONICA SINICA], 1992, No 6 [translated in full in JPRS-CST-92-023, 19 Nov 92 pp 19-24].
2. Desai, M., et al., "Convolution Back-Projection Image Reconstruction for SAR," ISCAS'84.
3. Huang, TS., et al., "Iterative Image Restoration," APP. OPT., 1975, 14.
4. Hopfield, J. J., Tank, D. W., "Neural Computation of Decision in Optimization Problems," BIOLOGICAL CYBERNETICS, 1985, 52.
5. Jha, S., et al., "Bearing Estimation Using Neural Networks," ICASSP'88.
6. Goryn, D., Kaveh, M., "Neural Networks for Narrowband and Wideband Direction Finding," ICASSP'88.
7. Rastogi, R., et al., "Array Signal Processing With Interconnected Neuronlike Elements," ICASSP'87.

Nation's Largest Trans-Supersonic Wind Tunnel To Be Completed in '96

94P60070A Chengdu SICHUAN RIBAO in Chinese
19 Nov 93 p 1

[Text] Work on the Mianyang China Aeropropulsion Research and Development Center's experimental trans-supersonic wind tunnel has begun. The project, now in its early stages, involves a supersonic wind tunnel section measuring 2.4 m x 2.4 m. Plans call for the wind tunnel to be operational in 1996. It will be the largest in China or, for that matter, in Asia. It will fill a void in trans-supersonic wind tunnel research as China does not possess such a facility above 2 meters at present. The facility will promote China's aerodynamic research. .

Two Dimensional Prediction for Solid Propellant Rocket Motor Internal Flowfield During Starting Transients

40100024A Beijing YUHANG XUEBAO [JOURNAL OF ASTRONAUTICS] in Chinese
Vol 14 No 4, Oct 93 pp 8-15

[English abstract of article by Song Mingde, Jian Zequn, Wang Jingchao, and Ye Dingyou, P.O. Box 169, Xi'an, 710000]

[Text] Internal flow during starting transient process was analyzed with 2D, inviscid, unsteady, compressible model. MacCormack's two-step explicit finite difference scheme is adopted for the solution of the Euler governing equations. The distribution of pressure, temperature and velocity has been predicted with this model. Also a new equal volume approximate technique was presented to analyze the internal flowfield in 3D grain post during the ignition process.

Subject terms: Solid propellant rocket motor, Starting transients, Internal flowfield.

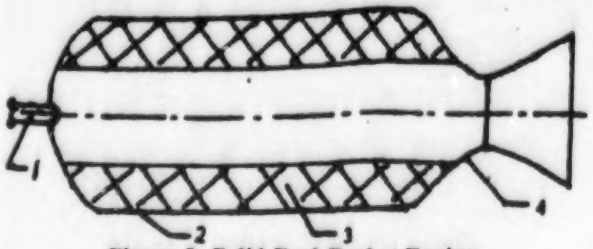

Figure 2. Solid-Fuel Rocket Engine.

1. Ignition system; 2. Hull; 3. Propellant; 4. Nozzle

Applications of Variable Structure Method to Missile Control

40100024B Beijing YUHANG XUEBAO [JOURNAL OF ASTRONAUTICS] in Chinese
Vol 14 No 4, Oct 93 pp 29-34

[English abstract of article by Zhang Jia-yu of the Harbin Institute of Technology and Lian Jin-bo of Institute of No. 710, Ministry of Aero-Space Industry]

[Text] In this paper, aiming at the parameters varing [as published], the variable Structure Control method is applied. By some design skill, the chattering is suppressed. When control is constrained, a method is developed to improve response speed. The simulation results of XX missile show that the method is effective. The system has strong adaptability to the variable of parameters and has high performance.

Subject terms: Variable structure control; sliding mode; anti-warship missile control; control constrained.

On the Large-Scale Amplitude Sloshing Dynamics of Liquid-Filled System Under Low-Gravity Environments and Its Applications in Space Technology

40100024C Beijing YUHANG XUEBAO [JOURNAL OF ASTRONAUTICS] in Chinese
Vol 14 No 4, Oct 93 pp 35-40

[English abstract of article by Wang Zhaoling of Tsinghua University and Zhang Naigong of the Chinese Academy of Sciences]

[Text] In this paper the theoretical foundation of large-scale amplitude sloshing dynamics of liquid-filled system is expounded under low-gravity environments. Then, its applications are clarified in the field of dynamics and control of spacecraft filled with liquid. Finally, the free boundary determination of large-scale amplitude sloshing and the numerical stability of data are analyzed.

Subject terms: Large-scale amplitude sloshing, Low-gravity, Sloshing suppression, Free boundary, Space shuttle, Aero-space shuttle.

Dose Measurement and Analysis of Space Radiation in the Cabins of the Recoverable Satellites

40100024D Beijing YUHANG XUEBAO [JOURNAL OF ASTRONAUTICS] in Chinese
Vol 14 No 4, Oct 93 pp 56-60

[English abstract of article by Qi Zhangnian, Chen Mei, and Li Xianggao of the Institute of Space Medico-Engineering, Beijing 100094]

[Text] Several measured radiation doses on board our nation's recoverable satellites were presented. The effects of orbit altitude and shield mass thickness on dose were analyzed. The complex shielding in the cabins of the satellites causes variations in the dose as a function of location. The measured results showed a dose maximum/dose minimum variation of 1.58 at the -500 km, of 1.23 at the -300 km. The radiation risk and protection during manned missions in low Earth orbit were discussed.

Subject terms: space radiation, radiation dose, radiation protection.

CAS Develops High-Altitude Balloon Microgravity Experimental System

94P60090 Beijing ZHONGGUO KEXUE BAO [CHINESE SCIENCE NEWS] in Chinese
15 Dec 93 p 1

[Text] Recently the Space Sciences Applied Research Center of the Chinese Academy of Sciences successfully developed a balloon microgravity experimental system, a high-technology project under the State's '863' program.

The balloon microgravity experimental system is a simulated space microgravity environment facility. It employs a high-altitude balloon to drop a capsule to produce a microgravity environment. Under this short-duration microgravity environment, experiments may be conducted in the materials, life, and fluid sciences, tests made on fuels, etc. Tests may also be conducted on the experimental payloads that are carried on satellites or airships.

The microgravity experimental system developed by the Space Center releases a drop capsule from altitudes of approximately 35 kilometers so that a microgravity environment of 10^{-4}g to 10^{-2}g can be maintained in free fall a period of 31 seconds.

The systems engineering tests and first lift test (a dust explosion characteristic test) were completely successful. The system weighs a total of 275 kilograms. All on-board instruments functioned normally, control was without error and the data acquisition systems obtained all necessary engineering test data and lift experimental data. The recovery of the system went off without incident and the system was ready for re-use.

China is now the third nation (following Japan and Germany) to develop this kind of microgravity experimental system.

Activities of Satellite Simulation Center Detailed

94FE0093A Beijing ZHONGGUO HANGKONG HANGTIAN BAO [CHINA AEROSPACE NEWS] in Chinese No 9, Sep 93 pp 3-7

[Article by Lin Laixing [2651 0171 5281]]

[Text] In order to satisfy China's needs for future development of various types of satellites, a decision was made in 1984 to build the Satellite Simulation Center (SSC). The main function of the SSC was to perform

semi-physical simulation tests of the control systems of high-orbit satellites and mid/low-orbit satellites. In the area of full-physical simulation, a single-axis air-float type platform system was constructed, and efforts were devoted to the research and development of full-physical simulation techniques.

The construction of the SSC was completed in two stages. The first stage was devoted to the construction of the high-orbit satellite simulation laboratories and some other facilities. At the end of 1989, a three-story, 2,700-square-meter simulation building was completed. The building contains five different simulation laboratories. On the first floor, there are two semi-physical simulation laboratories designed for high-orbit and low-orbit satellites and an air-float type platform simulation laboratory; the second floor contains the simulation computer laboratory (including CAD); the third floor contains the real-time data-transmission work station and the test laboratory for products and simulation equipment. By 1991, the development, installation, testing and operation of all simulation equipment planned for the first-stage construction were completed; the first semi-physical simulation test of the high-orbit satellite attitude control system was conducted in October 1992.

I. Satellite Simulation System

1. Design Concept of the Satellite Simulation System

(1) To apply advanced simulation techniques to the development process of satellite systems (particularly control systems), which includes design verification, preliminary design, prototype and product development, as well as post-launch on-orbit operation.

(2) To develop practical mathematical, semi-physical and full-physical simulation techniques and to incorporate these techniques in an integrated system.

(3) To apply different but complementary simulation techniques at different stages of development in order to achieve maximum effect from simulation.

(4) To establish a unified plan for utilizing the simulation test facilities; to construct simulation laboratories according to a systematic and coordinated test plan and to avoid duplicated efforts.

2. Functions of the Satellite Simulation System

The main functions of the satellite simulation system include: mathematical simulation, semi-physical and full-physical simulations of the satellite control system, semi-physical simulation of the onboard computer system and mathematical simulation of satellite orbits. The specific functions are described below.

(1) Feasibility study and design of satellite control systems using computers. Simulation computers are equipped with special software packages to perform mathematical simulations and system design of different types of control systems and to provide optimum design parameters.

(2) Semi-physical and full-physical simulations are performed on systems built from existing and newly developed components in order to verify and evaluate the control system's dynamic performance.

(3) Closed-loop simulation tests. The developed control system (both prototype and final product) is first subject to integrated (or open-loop) tests; then its performance is verified and evaluated through closed-loop physical simulation tests to determine if the system meets design specifications.

(4) Simulation of fault occurrence and fault-recovery strategies. Fault occurrences in satellite control systems can be simulated either mathematically or physically. Through simulations one can study the system behavior under different fault conditions and strategies for correcting the faults.

(5) Real-time display, collection and processing of flight test data. Real-time data received from the satellite tracking stations or small telemetry antennas are projected onto a screen by the data transmission work station in order to monitor the on-orbit operating conditions of the satellite. These data can be collected simultaneously by the data pre-processing system and sent to the simulation computer for real-time or off-line processing.

(6) System model verification. Through system simulations and flight tests, experimental data are collected and used to verify and modify existing mathematical models or to establish new models; these models include the noise model and interference model of different sensors, the pass-zero torque model of the flywheel system, the elasto-dynamic model of the solar panel, and the liquid sloshing model of the propellant tank.

(7) Onboard computer simulation. The onboard computer simulator can be used to perform software simulation design; the onboard computer and ground simulation computer can also be used to verify the hardware and software performance of the onboard computer.

(8) Mathematical simulation of satellite orbit.

3. Organization of the Satellite Simulation System

The satellite simulation system consists of two major segments: hardware (which includes the laboratories, the simulation equipment and the simulation computer) and software; the specific items in each segment are shown in the following chart. There are five simulation laboratories in the satellite simulation system; the equipment contained in each laboratory are shown in Figure 1.

(1) Simulation Computer Laboratory

The main computers include an Encore computer and a VAX-11/750 computer with simulation work stations. They are primarily used for real-time mathematical and semi-physical simulations and for research and design of satellite control systems.

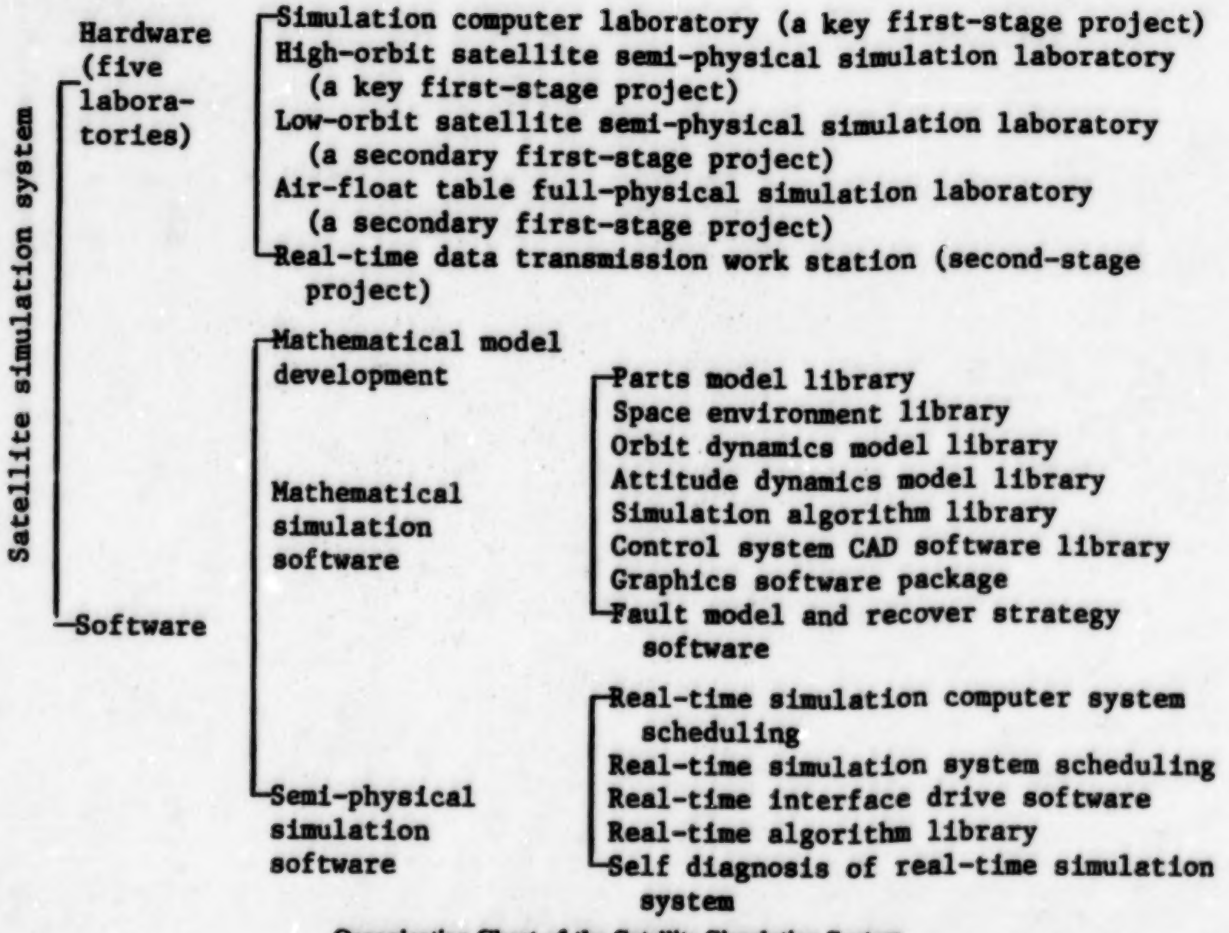

Organization Chart of the Satellite Simulation System

(2) High-Orbit Satellite Semi-Physical Simulation Laboratory

This laboratory is designed to perform semi-physical simulations of the process of establishing attitude for geosynchronous spin-stabilized and three-axis stabilized satellites during the period from satellite separation to apogee-motor ignition and of the attitude control system for geosynchronous-orbit operation.

(3) Low-Orbit Satellite Semi-Physical Simulation Laboratory

This laboratory is designed to perform semi-physical simulations of the control systems of mid and low-orbit three-axis stabilized satellites (including sun-synchronous orbits) with various attitude sensors. Specifically, it simulates the operation of the attitude control system during the entire process of orbit injection, initial attitude adjustment, orbit operation and programmed turn prior to recovery. Because of the non-uniform operating conditions of different sensors, they are installed on different turntables which are controlled and synchronized by the simulation computer.

(4) Air-Float Full-Physical Simulation Laboratory

The full-physical simulation laboratory is designed to perform satellite dynamic simulation using air-float platforms; its objective is to verify the performance of control systems equipped with inertial devices (e.g., flywheels, bias momentum wheels and control torque gyros, etc.). The main equipment of this laboratory include a single-axis air-float platform and a three-axis air-float platform, as shown in Figure 2 [photo not reproduced]. This laboratory can also perform dynamic simulation of the satellite's flexible structures such as the solar panel.

(5) Real-Time Data Transmission Work Station

The main function of the real-time data transmission work station is to monitor and collect information on satellite parameters during launch. The satellite parameters are provided by the satellite tracking station via co-axial cables and by the telemetry data received by the small telemetry antenna. The parameters are projected onto a large TV screen and are sent to the data processing system to generate attitude information and other

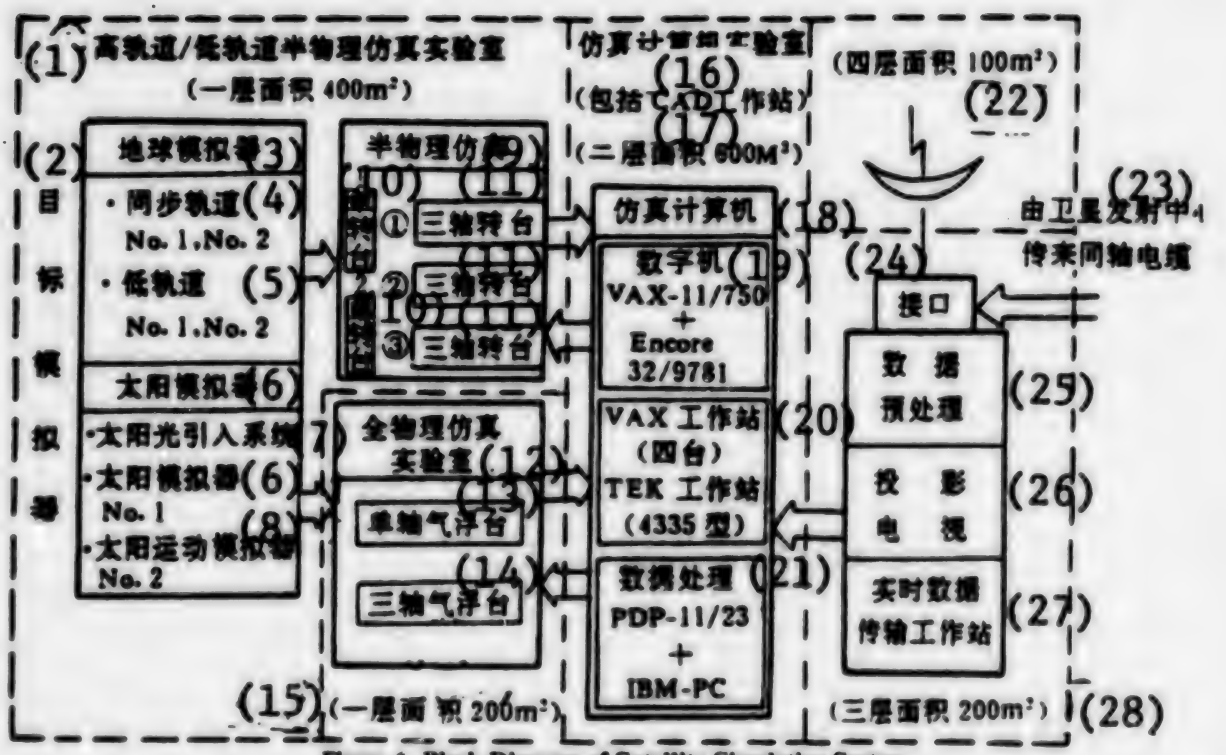

Figure 1. Block Diagram of Satellite Simulation System

Key: 1. High-orbit/low-orbit semi-physical simulation laboratory (first-floor area 400 m^2); 2. Target simulator; 3. Earth simulator; 4. Geosynchronous orbit; 5. Low orbit; 6. Sun simulator; 7. Sunlight capture system; 8. Solar-motion simulator; 9. Semi-physical simulation; 10. Single-axis turntable; 11. Three-axis turntable; 12. Full-physical simulation laboratory; 13. Single-axis air-float platform; 14. Three-axis air-float platform; 15. (first-floor area 200 m^2); 16. Simulation computer laboratory (including CAD work station); 17. (second-floor area 600 m^2); 18. Simulation computer; 19. Digital computers VAX-11/750 + Encore 32/9781; 20. VAX work stations (4), TEK work stations (model 4335); 21. Data processing PDP-11/23 + IBM PC; 22. (fourth-floor area 100 m^2); 23. Co-axial cable from the satellite launch center; 24. Interface; 25. Data pre-processing; 26. Projection television; 27. Real-time data transmission work station; 28. (third-floor area 200 m^2)

related information. The useful data from the flight test are stored in a data library which can be retrieved to support future research and design activities and fault analysis of satellite control systems.

II. Semi-Physical Simulation Experiments of Satellite Attitude Control Systems

During the past few years, the SSC has conducted semi-physical simulation experiments of the control systems of four different models of geosynchronous communications satellites; these experiments provided the necessary data to verify the control system design and the performance at various stages of operation; they also provided the experimental data for design improvement.

1. Semi-Physical Simulation Experiment of the Attitude Control System of Geosynchronous Communications Satellites

To meet the overall attitude-control requirements of communications satellites, semi-physical simulation experiments have been designed to accomplish the following tasks:

(1) To study and verify the attitude determination process (including geometric attitude determination and Kalman Filter process) during the transfer orbit, and to verify the design and accuracy of the attitude determination procedure.

(2) To verify the performance of the de-spin system under nutation conditions and the accuracy of the Earth-pointing system.

The main equipment used for this experiment is shown in Figure 1 on the inside front cover [photo not reproduced].

2. Semi-Physical Simulation Experiment of the Attitude Control System of Earth Observation Satellites

To meet the overall attitude-control requirements of Earth observation satellites, semi-physical simulation experiments have been designed to accomplish the following tasks:

(1) To verify the control process to accomplish initial attitude adjustment.

(2) To verify the Earth-pointing accuracy of the attitude control system with and without correction of gyro drift using sun sensors.

(3) To predict the performance of the control system when the satellite attitude undergoes large changes.

Significant improvements have been made in simulation techniques, particularly in the following three areas:

A. By using fully digital real-time simulation techniques, high accuracy and good repeatability have been achieved.

B. By using multiple turntables, the field-of-view requirements of different sensors are satisfied with no blockages; also, full-orbit simulation capability is achieved.

C. By using onboard computers, it is possible to test not only the hardware components of the control system but also the software design in the simulation laboratory.

The main equipment used for this experiment is shown in Figure 2 on the inside front cover [photo not reproduced].

3. Semi-Physical Simulation Experiment of the Active Nutation Control System of Spinning Satellites

Because of energy dissipation caused by the motion of flexible parts and liquid inside the satellite, a spinning satellite is stable only if it spins about an axis of maximum inertia. To achieve stability, the satellite should have a longitudinal-to-lateral inertia ratio greater than 1. But in many cases this condition cannot be met (for example, a slender satellite body), then the nutation angle of the satellite (the angle between the spin axis and the angular momentum vector) will grow with time. In order to ensure satellite stability, an active nutation control system must be used; such a system uses an accelerometer to measure the nutation angle and a jet device as the actuating mechanism. A block diagram of the semi-physical simulation experiment of the active nutation control system is shown in Figure 3.

The main objectives of this experiment are:

(1) To verify the feasibility of using accelerometer to measure the nutation angle of spinning satellite.

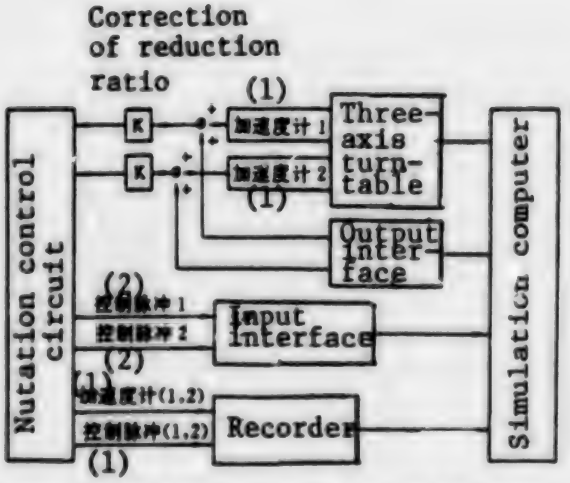

Figure 3. Block Diagram of Semi-Physical Simulation Experiment of Active Nutation Control System

Key: 1. Accelerometer; 2. Control pulse

(2) To verify the validity of fine control logic and coarse control logic of the controller under small and large nutation angles.

(3) To verify the design and performance of the active nutation control circuit (the time required for the initial nutation angle to vanish and the control accuracy).

(4) To investigate the interference effects of nutation control on attitude stability.

This experiment has provided verifications of the feasibility of using accelerometer for nutation measurement and the feasibility of fine and coarse active nutation control design. In addition, simulations of various control parameters have provided results that show the effects of these parameters on the performance of the control system; such results can be used for future design improvements.

4. Semi-Physical Simulation Experiment of the Attitude Control System of High-Orbit Satellites

The satellite used for this experiment is a three-axis stabilized, geosynchronous broadcast satellite which has an Earth-pointing accuracy of 0.1°-0.15° and an operating life of 8 years. This is a Chinese-built satellite with state-of-the-art technology. In order to ensure good performance and operational reliability of the control system, semi-physical simulation experiments have been carried out for eight different modes of the attitude control system:

(1) The speed damping + Sun acquisition mode (A);

(2) The Sun acquisition mode (B);

(3) The Earth acquisition and Earth pointing mode;

(4) The apogee motor ignition mode;

(5) The position-keeping (fixed point acquisition mode);

(6) The transition mode;

(7) The normal mode;

(8) The malfunction mode.

The main equipment used for this experiment is shown in Figure 3 on the inside front cover [photo not reproduced].

III. Multiple Turntable Semi-Physical Simulation System

One of the main projects of the second-stage construction of the Satellite Simulation Center is to develop and build a multiple turntable semi-physical simulation system to satisfy the simulation needs of various sensors and actuating mechanisms.

The main requirements for modern applications satellites are high accuracy and extended operating life; such satellites rely on different types of sensors (Sun sensors, infrared sensors, starlite sensors, gyros) and multiple actuating mechanisms (flywheels, jets and magnetic torques) for attitude control. In order to accommodate these different sensors and actuating mechanisms in a closed-loop simulation circuit, the SSC has developed a multiple turntable semi-physical simulation system.

Figure 4 shows a block diagram of such a simulation system. It is seen that the simulations of several commonly used attitude sensors are accomplished by the SSC's 5 turntables. The simulation of the Sun sensor, the star sensor and the gyro (or the accelerometer) is accomplished by a three-axis turntable; the pitch and roll motions of the low-orbit infrared horizon sensor are simulated by two single-axis turntables so that the large Earth angle seen by the low-orbit satellite can be accommodated. For a geosynchronous satellite which has a much smaller Earth-view angle, the infrared horizon sensor and the gyro can share a common three-axis turntable.

The most difficult problem in simulating actuating mechanisms is to simulate the magnetic torque. Because

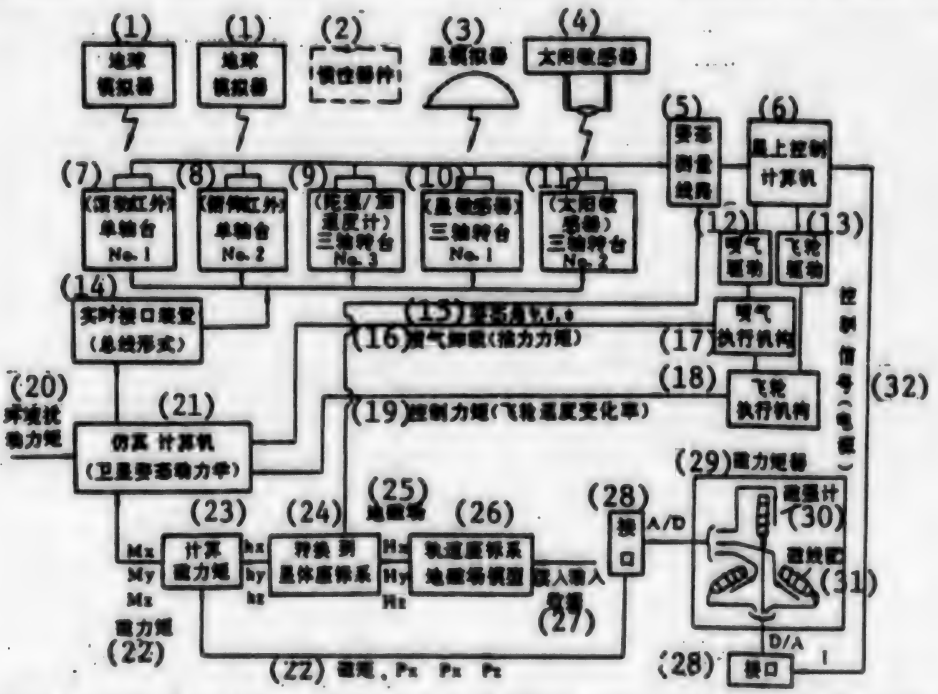

Figure 4. Block Diagram of the Multiple Turntable and Multiple Actuating Mechanism Semi-Physical Attitude Simulation System

Key: 1. Earth simulator; 2. Inertial devices; 3. Star simulator; 4. Sun sensor; 5. Attitude measurement circuit; 6. Onboard control computer; 7. (Roll infrared) single-axis turntable No. 1; 8. (Pitch infrared) single-axis turntable No. 2; 9. (Gyro/accelerometer) three-axis turntable No. 3; 10. (Star sensor) three-axis turntable No 1.; 11. (Sun sensor) three-axis turntable No. 2; 12. Jet drive; 13. Flywheel drive; 14. Real time interface bus; 15. Attitude angles (φ, θ, ψ); 16. Jet-produced thrust torque; 17. Jet actuating mechanism; 18. Flywheel actuating mechanism; 19. Control torque (rate of change of the flywheel speed); 20. Disturbance torque; 21. Simulation computer (satellite attitude dynamics); 22. Magnetic torque; 23. Magnetic torque computation; 24. Transformation to satellite body coordinate system; 25. Geomagnetic field; 26. Orbit coordinate system, geomagnetic field model; 27. Read input data; 28. Interface; 29. Magnetic torque device; 30. Magnetometer; 31. Magnetic coil; 32. Control signal (power source)

of the non-linearity of the magnetic hysteresis circuit and the complexity of its behavior, it cannot be accurately described by simple mathematical expressions. To solve this problem, the SSC has proposed a digital model of the geomagnetic field from which accurate simulation of the magnetic torque can be achieved. The geomagnetic field components of the satellite attitude along each axis of the orbit coordinate system (H_x, H_y, H_z) can be determined from the actual orbital position of the satellite; this field vector can then be transformed into the satellite body coordinate system (h_x, h_y, h_z) based on the instantaneous attitude angles (φ, θ, ψ). The magnetic torque of the actuating mechanism can be measured accurately in real time using a magnetometer.

The torque produced by the flywheel can be determined by measuring the rate of change of the speed of the flywheel, which is connected to the simulation circuit. The jet actuating mechanism can produce a thrust torque which depends on the performance curve of the electromagnetic valve.

In semi-physical simulations using multiple turntables and multiple actuating mechanisms, the turntables and the control equipment are linked together synchronously by interface bus lines. Of course, it is possible to link only a selected number of turntables or target simulators based on satellite attitude control needs.

With the completion of the multiple-turntable semi-physical simulation system, preparation time for future simulation experiments can be reduced from one or more years to only a few months; it would also be possible to perform full-orbit simulation with significantly enhanced accuracy and fidelity.

IV. Conclusion

Operational experience with the SSC has shown that the design and layout, the technical performance and reliability of the satellite simulation system have met the requirements for conducting simulation experiments of various satellite control systems. Using state-of-the-art simulation techniques, the SSC has played an important role in the development of future satellite models.

Study of Zirconia-Toughened Cordierite Ceramics (ZTCC)

40100020A Beijing GUISUANYAN XUEBAO [JOURNAL OF THE CHINESE CERAMIC SOCIETY] in Chinese Vol 21 No 5, Oct 93 pp 399-405

[English abstract of article by Wu Jiezheng, Chen Yuqing, and Wang Lianxing of the Northwest Institute of Light Industry, Xianyang, Shanxi Province 712081; MS received 14 Apr 92]

[Text] Strengthening and toughening of polycrystalline cordierite ceramics added with different amounts of ZrO_2 dispersed particles are investigated. Synthetic highly pure cordierite (HPC) (1400°C, 6h) has a very low linear thermal expansion coefficient of 1.54 x 10^{-6}/°C, a flexural strength of 74.3 MPa and a fracture toughness of 1.60 MPa-$m^{1/2}$. The flexural strength can be increased to 130 MPa by adding 10 percent (in mass) ZrO_2 dispersed particles in ZTCC, and the fracture toughness of ZTCC with added 5 percent (in mass) ZrO_2 and 1 percent (in mass) CaO dispersed particles arrives at a level of 2.83 MPa-$m^{1/2}$. The effects of strengthening and toughening by adding superfine 15 percent (in mass) Y-TZP dispersed particles on ZTCC are so remarkable that the flexural strength and fracture toughness can be increased to 188 MPa and 3.2 MPa-$m^{1/2}$, respectively, which implies that the increase of strengthening and toughening is 153 percent and 100 percent, respectively. The main toughening mechanism of ZTCC is crack deflection and microcracking. ZTCC containing ZrO_2 dispersed particles has the same thermal shock resistance as HPC ceramics, while ZTCC shows better thermal shock resistance by addition of ZrO_2 and CaO dispersed particles. It seems that ZTCC is suitable for use as a thermal-shock-resistant material because of its low thermal expansion and relatively good mechanical properties.

Preparation of Aluminum Nitride Powder Under Pressurized Nitrogen Atmosphere

40100020B Beijing GUISUANYAN XUEBAO [JOURNAL OF THE CHINESE CERAMIC SOCIETY] in Chinese Vol 21 No 5, Oct 93 pp 457-460

[English abstract of article by Luo Xinyu, Zhuang Hanrui, et al. of the Shanghai Institute of Ceramics, Chinese Academy of Sciences, Shanghai 200050; MS received 14 Jan 92]

[Text] The preparation of aluminium nitride powder by means of direct nitridation under pressurized nitrogen atmosphere and carbothermal nitridation of alumina is studied. The results show that aluminium nitride powder can be synthesized by accelerated nitridation at high temperature and high pressure. The critical temperature is 700°C and the critical pressure is 1 MPa (N_2). Aluminium nitride powder can be synthesized also by carbothermal nitridation in nitrogen at high pressure. The nitrogen content of aluminium nitride powder depends on the soaking temperature, the nitrogen pressure and the soaking time. Under pressurized nitrogen atmosphere, aluminium powder can be used as the seed of aluminium nitride powder by carbothermal nitridation of alumina. High-quality aluminium nitride powder can be obtained by this method.

Hypervelocity-Impact-Resistant Composites Developed, Tested

94FE0068A Beijing GAO JISHU TONGXUN [HIGH TECHNOLOGY LETTERS] in Chinese Vol 3 No 6, Jun 93 pp 5-8

[Article by Liu Fengrong [0491 7685 2837], Su Bo [5685 3134], Wu Xiaojin [0702 1420 6651], and Wang Xingye [3769 5281 2814] of National University of Defense Technology, Changsha, 410073: "Hypervelocity-Impact-Resistant Composite Materials," funded by 863 Plan; MS received 19 Feb 93]

[Text]

Abstract

This article discusses the design, preparation, and testing of hypervelocity-impact-resistant composites. The areal density of the composites is 1.96-2.60 g/cm^2. The projectiles used for testing are 5-mm-diameter aluminum balls. The testing speeds of the projectiles vary from 2.81 km/s to 7.81 km/s. The composites have proven quite satisfactory in resisting the hypervelocity projectiles when tested under the experimental conditions for the double-sheet structure.

Key words: hypervelocity impact, composite material.

I. Introduction

Hypervelocity-impact-resistant materials are important protective materials for space vehicles and modern military equipment. As early as the 1950s, the problems of impacts between micrometeors and space vehicles were researched internationally. Since the 1960s, development of space activities has accelerated, and fragments from failed space vehicles left in orbit have increased at a rate of 5 percent yearly. These fragments endanger orbiting space vehicles, especially manned ones.[1,2] In the 1980s, the United States, Western Europe, and Japan began R&D of long-duration manned space stations, and explicitly demanded protection from the impacts of micrometeorites and orbiting debris.[3] Important developments in kinetic-energy-resistant materials have been achieved in the United States. In 1988, the development of a "low-density multilayer shield" capable of resisting high-velocity bullets was reported. This paper presents the design, preparation, and testing of a multilayer composite that is hypervelocity-impact-resistant.

II. Design of Hypervelocity-Impact-Resistant Composites

Current studies show that the best design is the stand-off multiple-layer structure suggested by F. L. Whipple in 1952.[4] For practical purposes, the design always uses the double-layer shield structure, which consists of three components: the shield target-plate, the main target-plate, and the gap between the two plates. When a projectile hits the shield plate, the impact force transforms the projectile into solid particles, molten metal drops, and gaseous materials. The three phases mix together and form a "fragment-cloud-cluster." The cluster expands in the gap and collides onto the main target-plate (Figure 2).

Existing research papers conclude that the fragment-cloud-cluster damages the main target-plate in the following modes: heat ablation, pit erosion, layer cracking, and penetration. Combining the theoretical model and some distinguished properties of different composites, we have designed a multilayer composite with a ceramic-matrix composite as the protective layer, a porous variable-density composite material as the buffer layer, and a woven composite as the structural layer.

III. Manufacturing of Composite With Multilayer Structure

1. Protective Layer

The SiC composite has the distinguished properties of high hardness, high strength, heat resistance, etc. The precursor (polycarbosilane) transformation method is used to prepare the continuous CF/SiC, segmental CF/SiC, and SiC_p/SiC (Figure 1 shows the preparation method). We first compare the strength, hardness and heat-resistance properties as well as the technological requirements of these three materials, then we study the hypervelocity-impact-resistance function of the protective layer. Based on the above considerations, we select SiC_p/SiC as the protective layer material. The room-temperature bending strength of SiC_p/SiC reaches 350 MPa; and at 1300°C, 300 MPa. Its Vickers hardness is HV30 = 435 kg/mm^2.

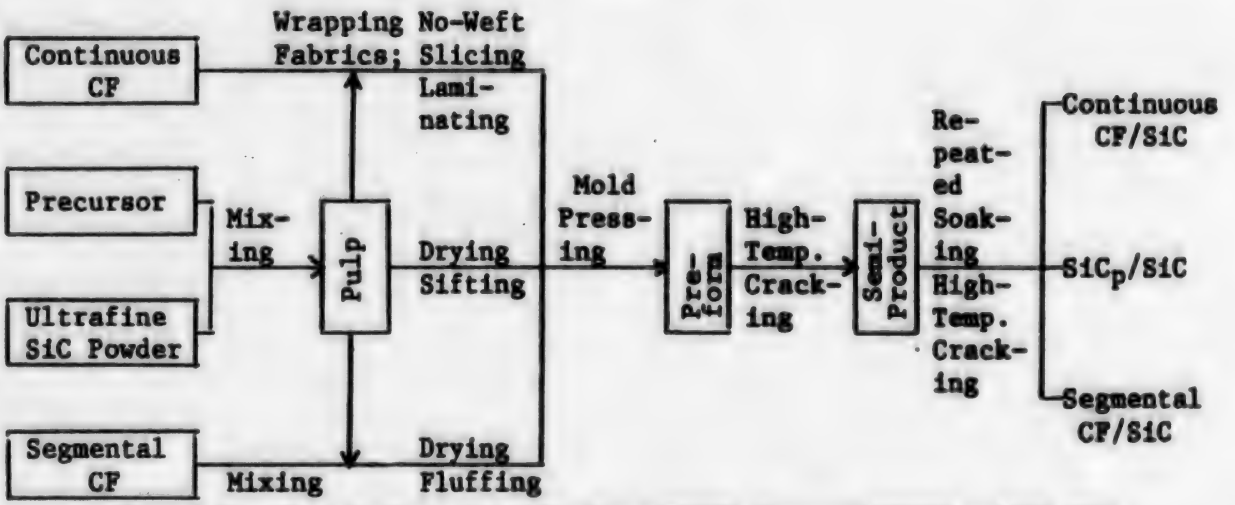

Figure 1. Flow Chart for Preparation of Continuous CF/SiC, Segmental CF/SiC, and SiC_p/SiC

2. Buffer Layer

A hollowed-Al_2O_3-pellet/epoxy is used for the buffer layer. The fabrication method is as follows: Hollowed alumina pellets are classified, surface-treated, and mixed with an epoxy base. The mixture is solidified by press molding. The density of the mixture is 1.13 g/cm^3; porosity, 45 percent; and compressive strength, 38.8 MPa.

3. Structural Layer

The structural layer is the main body of the hypervelocity-impact-resistant composite. Glass-fiber and carbon-fiber-woven materials with epoxy (3DB G/EP and 3DB C/EP, respectively) are used. Each woven material is first soaked (with epoxy?) in vacuum, and then solidified in a heated mold under pressure. The property parameters of the two basic woven materials and the properties of the corresponding composites are given in Tables 1 and 2, respectively.

Table 1. Woven Material Property Parameters

Woven material	3DB-G	3DB-C
Parameters		
Woven technique	4-step method	4-step method
Fiber number	12K	12K
Fiber density (g/cm^3)	2.54	1.76
Fiber strength (MPa)	2900-3300	2400-2700
Fiber volume fraction (%)	48	40

Table 2. Woven Composite Mechanical Properties

Composites		3DB-G/EP	3DB-C/EP
Properties			
Tensile strength (MPa)		—	362
Tensile modulus (GPa)		—	362
Compressive strength (MPa)	X	149.6	50.5
	Y	151.8	88.1
Bend strength (MPa)		254.2	126.0
Bend modulus (GPa)		4.28	6.82

Additionally, a porous variable-density 3DB C/EP composite is made under controlled conditions. The average density of the front half layer is 1.11 g/cm^3; and that of the rear half layer, 1.30 g/cm^3. The variable-density composite can eliminate the hollowed-Al_2O_3-pellet/epoxy buffer layer.

The multilayer composite is made by consolidating the protective layer, buffer layer, and structural layer.

IV. Experimental Results and Discussion

The hypervelocity impact test is conducted with a two-stage cannon. The projectiles are 5-mm-diameter hard aluminum balls. The test velocities are in the 2.81-7.81 km/s range. Figure 2 shows the test arrangement, while Table 3 shows the test results.

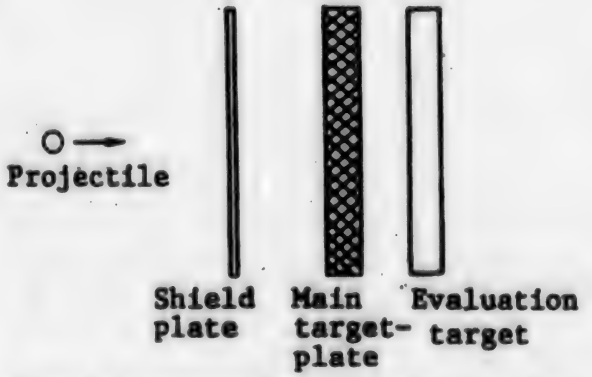

Figure 2. Arrangement for Hypervelocity Impact Test

Table 3. Hypervelocity Impact Test Results of Multilayer Composite

Multilayer composite	Areal density (g/cm^2)	Projectile velocity (km/s)	Damages	
			Protective layer and buffer layer	Back of structural layer
I	2.30-2.60	4.36-7.02	Different degrees of crumbling in buffer layer in the eroded area (diameter 25-33 mm)	Basically in good condition
II	2.43-2.59	5.25-7.81	Different degrees of crumbling in heavily eroded area (diameter 32-41 mm)	Basically in good condition
III	1.96-2.34	2.81-6.56	Almost all of protective layer crumbles in heavily eroded areas (diameter 25-32 mm)	Basically in good condition

The main criterion to evaluate the hypervelocity-impact-resistant properties is the degree of damage on the surface and the back of the material. Table 3 shows that among the three composites, only the protective layers and the buffer layers suffer different degrees of erosion and crumbling. The low-density surfaces of the structural layers suffer slight damage; the back parts are essentially intact, as no damage is observed macroscopically. After testing, the appearances of these three composites do not show any obvious differences regardless of their construction differences. The results show that all three multilayer structural composites have good hypervelocity-impact-resistant properties.

Based on past papers, when the projectile velocity is below 4 km/s, the fragment-cloud-cluster contains more large solid particles and has stronger penetrating power, which consequently causes heavier damage on the main target-plate. In our experiment, although the velocities of the different projectiles vary from 2.81 km/s to 7.81 km/s, the experimental results do not show significant variations in damage, which indicates that our composites can resist projectiles with a broad range of impact velocities.

Another criterion to evaluate the composites is the residue strength after impact. Figure 3 shows the compressive strengths of the structural layers of two composites after the impact tests. It shows that the structural layers still maintain high residue stresses.

The damage characteristics and the residue strengths reveal the effects of hypervelocity impacts on the composite structures. The SiC_p/SiC protective layer has high hardness, high temperature resistance, good anti-erosion properties, and good heat-ablation resistance; however, it is brittle, and since the only way to attach it to the buffer layer is with adhesives, it crumbles easily. The buffer layer is made of hollowed-Al_2O_3-pellet/EP or a porous variable-density composite. During the course of shock-wave compression, these materials can absorb the energy. The structural layer of the 3DB C(G)/EP composite possesses the good properties of tear resistance, and crumble resistance; hence, after the hypervelocity impact, its back surface is essentially unchanged and also maintains high residue strength.

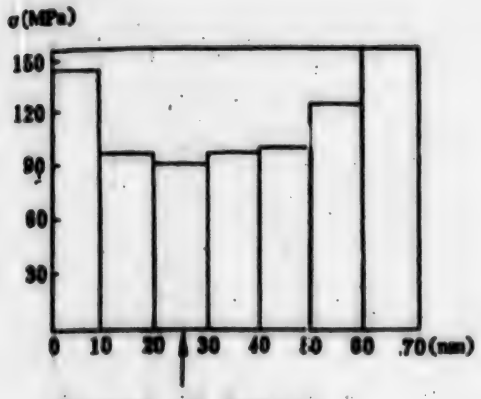

A. 3DB—G/EP

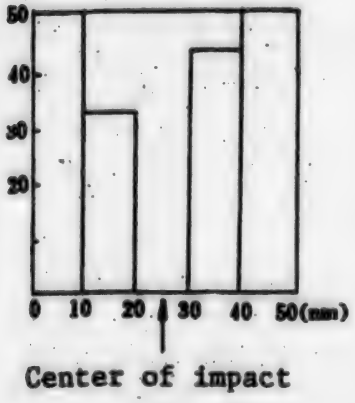

B. 3DB—C/EP

Figure 3. Composites' Residue Compressive Strength After Hypervelocity Impact Tests

V. Conclusions

1. The experiment shows that the multilayer composites made of SiC ceramic composite as the protective layer, hollow pellet or porous composite as the buffer layer, and woven material composite as the structural layer are very effective in resisting hypervelocity impact.

2. The hollowed-Al_2O_3-pellet/EP and porous variable-density 3DB/EP can weaken the stress wave.

3. All three multilayer composites have the characteristics of low areal density, resistance to a broad range of impact velocities, and good impact resistance.

Acknowledgment

The authors are grateful to Professor Zhang Ruoqi of the National University of Defense Technology for his assistance in the multilayer composite design.

References

1. N71-25070, "NASA Space Vehicle Design Criteria (Structures), Meteoroid Damage Assessment," May 1970.

2. Ernst Bauer, "Meteoroid and Orbital Debris Protection Concepts," IAA 86-419, 1986.

3. Garry, S., Winkelhoff, E., "Key Structures Mechanical Issues of the European Space Station and Platform Program Columbus," ESA SP-289, January 1989.

4. Lawrence, R. J., INT. J. IMPACT ENGNG, 1987, 5: 541-461 [as published].

Ultrathin PMMA LB Films for X-Ray High-Resolution Lithography

94FE0068B Beijing GAO JISHU TONGXUN [HIGH TECHNOLOGY LETTERS] in Chinese
Vol 3 No 6, Jun 93 pp 18-21

[Article by Gu Ning [7357 1337], Lu Wu [7627 2976], Lu Zuhong [7120 4371 1347], and Wei Yu [7279 6877] of Wu Chienshiung Lab, Southeast University, Nanjing, 210018; Shen Haoying [3088 3185 3467] of Nanjing Institute of Electron Devices, Nanjing, 210016; Tian Chaoyang [3944 6389 2799], Kan Ya [7074 1246], and Liu Zewen [0491 3419 2429] of the National Synchrotron Radiation Laboratory, University of Science and Technology of China, Hefei, 230026: "Ultrathin Poly(-methylmethacrylate) LB Films for X-Ray High-Resolution Lithography"; MS received 7 Mar 93, revised 12 Apr 93]

[Text]

Abstract

This is the first report of research on X-ray lithography on Langmuir-Blodgett (LB) monomolecular layers as photoresists. Each layer is made by drawing at a force of 15 dynes/cm. The thickness of the photoresists made from PMMA LB layers varies from 8 nm to 6.3 nm. The exposure is made with a low-d. ∞ X-ray of 360 mA-min. A resolution of 0.2-0.3 μm is achieved. (The resolution is limited by the maximum resolution of the mask, which is 0.2-0.3 μm.) The potential of adopting LB films as photoresists to improve X-ray lithography resolution from submicron class to nanometer class is discussed.

Key words: X-ray lithography, Langmuir-Blodgett (LB) films, Resolution, Nanometer structure.

A crucial factor in developing optoelectronic devices is in the area of nanometer technology, including especially lithography and its technology. As the required lithography standards in line width and resolution have advanced from the micron to the submicron and even to the nanometer range, electron-beam lithography and X-ray lithography become more and more important.

The consensus is that it costs less to lithograph the mask first and then duplicate the pattern in the mask onto the photoresist of the chip with X-rays, compared with engraving the pattern directly onto the photoresist of the chip with an electron beam. The former method will greatly increase the production rate.[1] Photoresist research has always been a very important link to X-ray lithography development. The resolution of X-ray lithography depends not only on such factors as X-ray wavelength, intensity, developing technique, and lithographic technique, but also on the resolution of the X-ray exposure on and the developing of the photoresist.[2]

R. Feber et al. have suggested an ideal photoresist model.[3] The X-rays are orthogonally projected onto a photoresist which is composed of a group of resolution elements. A resolution element is defined as the smallest volume element that can be resolved after the photoresist is developed. Its standard denotation is δ x δ for area, and d for thickness, as shown in Figure 1. In a unit time period, the average dose of X-rays absorbed by each resolution element is expressed by the following equation:

$$\dot{n} = \frac{Einc}{Hv} \cdot A \cdot \delta^2 \qquad (1)$$

where Einc is the exposure intensity; Hv, the energy of every X-ray quantum; and A, the energy absorption rate of a unit photoresist area with thickness d. Assuming that the linear absorption coefficient is α, then A is expressed as:

$$A = 1 - e^{-\alpha d} \qquad (2a)$$

$$A \approx \alpha d \text{ (when } \alpha d << 1) \qquad (2b)$$

The factor limiting the X-ray photoresist resolution is

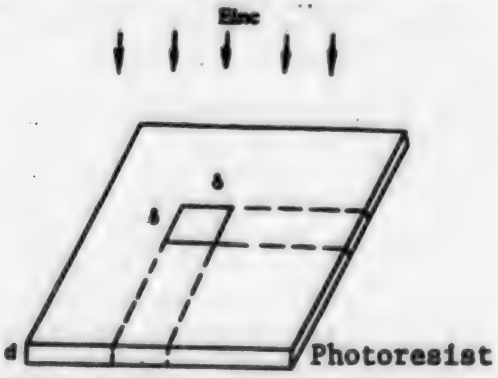

Figure 1. Resolution Element in Photoresist

dimension δ of the effective zone which can generate secondary electrons. The secondary electrons are the main motive force causing practically all the occurrences of the chemical reactions.[4] According to research results of E. Spiller et al., to improve the resolution to the maximum ($\delta \rightarrow \lambda$), the photoresist must be very thin, i.e., $d \approx \delta$.[5] Let us assume $d = \delta$; substituting the value into Equations (2b) and (1), we obtain:

$$Einc = \frac{\bar{n} \cdot h\nu}{\alpha \cdot \delta^3} \qquad (3)$$

We can see from the above that an ideal high-resolution photoresist should have low sensitivity. This requirement can also be applied to lithography in the micron and nanometer classes. As far as high-resolution photoresists are concerned, while the level of radiation remains unchanged, the process must be done under the condition of using corresponding ultrathin films. Based on this model, R. Feber et al. exposed PMMA photoresists with $d \approx 50$ Angstroms under the conditions $\lambda = 44.8$ Angstroms, $\bar{n} = 1.4$. They produced microscopic photographs of patterns with a nearly 50 Angstrom resolution in the nanometer class.[3]

Currently, photoresists are mainly made by the spinning method or the spray method. When making films of less than 50-nm thickness, these methods have the drawbacks of non-uniform thickness and high defect density; however, films of uniform thickness and considerably low defect density can be made with the LB film technique.[6] The technique is as follows: An organic material or polymer solution is spread on a sub-phase (e.g., water, glycerin, etc.) to form a monomolecular layer on the liquid surface. The layer is then transferred one after another onto a substrate and forms a solid ultrathin film with ordered molecular arrangement. Recently, many electron-beam photoresists have been made with LB films.[6,8] The LB film has definite future application in eliminating the "proximity effect" of the electron beam as well as producing nanoscale lithography patterns.[9]

The process to prepare LB films from poly(methylmethacrylate) or PMMA is as follows: First, the PMMA powder of molecular weight 1.8×10^5 (made by Huajin Company in Wuxi) is dissolved in trichloromethane ($CHCl_3$) forming a 0.5 mg/ml PMMA/$CHCl_3$ solution. The stable pure-water sub-phase in the Langmuir trough is made of super-pure water, twice distilled de-ionized water having electrical conductivity no higher than 10^{-8} $(ohm\text{-}cm)^{-1}$. The Langmuir trough is of the FACE type (made by Kyowa Kaimenkagaku Co. Ltd.). The PMMA/$CHCl_3$ solution is spread and forms a monomolecular layer on the sub-phase liquid. Figure 2 shows the curve plotted from the data of layer pressure and layer area (π - A). It reveals that PMMA forms a gas layer on the sub-phase liquid surface when the pressure is 2 dynes/cm; when the pressure is between 2 dynes/cm and 12 dynes/cm, the layer gradually transforms to a hybrid gas-liquid state. These properties are highly in line with the experimental results by Kuan et al.[10] Stoveve observes that when the film pressure is about 15 dynes/cm, the PMMA main chain is basically parallel to the gas-liquid interface and densely arranged on the liquid surface.[11] Hence, when we transfer the PMMA solid film to the substrate, we always maintain the pressure at 15 dynes/cm.

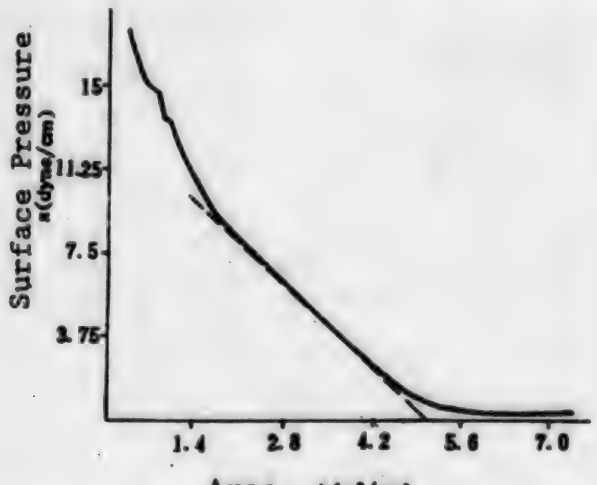

Figure 2. π - A of PMMA Curve

Pressure temperature, 14°C; PMMA molecular weight, 1.8×10^5

The chemically cleaned and hydrophobically treated Si chip is attached on the film extractor. The layer first extracted is baked at 100°C for 20 minutes to improve its adhesiveness to the chip; after that the extracting process is conducted in a continuous and vertical manner. After every 10 layers (up and down five times each way), the assembly is baked at 100°C for 10 minutes. Every PMMA layer is about 0.9 nm thick,[12] therefore the total thickness of the PMMA LB film transferred to the chip is the product of 0.9 nm and the number of layers. In the experiment under discussion, the total thickness of the PMMA LB photoresist for X-ray exposure is in the range of 1.8-6.3 nm.

The X-ray lithography test was conducted on the Si chips with PMMA LB films. The X-ray source is from the photolithography station of the synchrotron radiation accelerator in the State Synchrotron Radiation Laboratory operated by the University of Science and Technology of China. The wavelength of the X-rays ranges from 5 to 15 Angstroms; after filtering, from 5 to 10 Angstroms. The exposure area is 40 x 20 mm. The dose intensity is calculated as the product of accelerator tube current and exposure time, not counting the decaying current. Only one X-ray mask is used in the experiment. The maximum resolution is 0.2-0.3 μm (France). The developer is MIBK: IPA = 3:1 (20°C).

The X-ray exposure test shows that in the case of a PMMA LB film of about 36 to 63 nm thickness and 40 to 70 layers, good image quality can be achieved with an X-ray dose of 250 to 360 mA-min. The maximum mask resolution can be reproduced. In the case of a conventional film thicker than 1 μm made by the spinning method, an X-ray dose of 500 to 700 mA-min is needed for a quality image. Figure 3 shows three sets of grating images by a scanning electron microscope. Figure 3b shows the recurrence of the 0.2 to 0.3-μm maximum mask resolution. Figure 4 shows a different mask pattern, which is a checkerboard pattern developed after the X-ray exposure. Because the developer solution is too strong, the first 20-layer PMMA LB film does not reveal any image. Besides, any dose over 400 mA-min is also not suited for PMMA LB films with fewer than 70 layers.

Figure 3. SEM Photo of X-Ray Lithograph on PMMA LB Photoresist (a) Gratings of 3 different resolutions; (b) Resolution: 0.2 to 0.3 μm

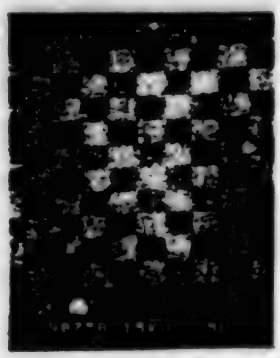

Figure 4. Developed SEM Photo of X-Ray Exposed PMMA LB Photoresist (checkerboard pattern)

Since lithography results depend also on other factors such as the composition of developer, the exposure time and other post-treatment techniques, the findings of this experiment, merely the results of our first trial, are deemed as preliminary; however, the experiment shows that there is a valid potential of making X-ray photoresists with LB films. The fact that the resolutions of the films progress from the micron to the submicron range, even to the nanometer range is especially important. Moreover, for the same resolution, employing the LB film can lessen the X-ray equipment requirement, e.g., reducing the demand on X-ray power, and eventually cutting down the cost. To overcome the problem wherein a thinner film leads to a weakening of the photoresist,

concrete technology may consider utilizing different resolutions and photoresist materials of varying film thickness to produce photoresists through the LB or other techniques. Another method to improve the photoresist property is to have the exposed photoresist layer undergo the self-rearranging growth measure. Further work on the project is now in progress.

References

1. Herriot, D. R., et al., IEEE TRANS., ED-22, 1975:385.
2. Dagneaux, P., et al., ANN. PHYS (Paris), 1975, 9:9.
3. Feder, R., et al., SCIENCE, 1977, 197:259.
4. Spear, D. L., et al., ELECTRON LETTERS, 1972, 8:102.
5. Queisser, H.-J., "X-Ray Optics, Applications to Solids," Springer-Verlag, 1977.
6. Barraud, A., et al., THIN SOLID FILMS, 1980, 68:91.
7. Hupfer, B., et al., MAKROMOL. CHEM., 1981, 182:247.
8. Cemel, A., et al., J. POLYM. SCI., 1972, A1-10, 2061.
9. Gu Ning, et al., Proceedings of First Conference on Functional Materials, Guilin, 1992, 10.
10. Kuan, S. W. J., et al., J. VAC. SCI. TECH., 1988, B5(6):2274.
11. Stroeve, P., et al., THIN SOLID FILMS, 1987, 146:209.
12. Zhang, H., et al., J. VAC. SCI. TECHNO., 1989, B7(6):1717.

Study of Modified Matrix Pitch for Carbon-Carbon Composite

94FE0068C Beijing GAO JISHU TONGXUN [HIGH TECHNOLOGY LETTERS] in Chinese
Vol 3 No 9, Sep 93 pp 7-8

[Article by Li Tiehu [2621 6993 5706], Yang Zheng [2799 1513], and Zheng Xiulin [6774 0208 7792] of the Materials Science and Engineering Department of Northwestern Polytechnical University, Xian, 710072: "Study of Pitch Property Modification for Matrix in Carbon/Carbon Composites"; MS received 11 Jun 93, revised 12 Jul 93]

[Text]

Abstract

Small-molecule materials in domestic industrial coal tar pitch are modified into large-molecule materials by the crosslinking catalytic method. Due to the increase of the C/H ratio in the molecules and high carbon yield rate, the compressive strength of the carbon/carbon composite is greatly improved.

Key words: Modified pitch, Crosslinking catalysis, Carbon-carbon composite.

I. Introduction

Pitches in general, and mesothermal pitch in particular, are a group of important precursors for the matrices of carbon/carbon composites. Their advantages are low cost and good fluidity, but they also have the drawbacks of low carbon yield rate, low strength, and low heat resistance. Therefore, research has focused on improving their properties. Laboratories in Japan have achieved important breakthroughs in simulating property improvement through the use of pure materials.[1] In the United States, industrial pitch is used as the raw material for property modification research;[2] however, it is hazardous to health and causes equipment damage. Based on numerous exploratory experiments, this study adopts the crosslinking catalytic method to modify the domestic mesothermal pitch. This method does not affect human health and equipment, and its low cost is economical for industrial promotion. The carbon/carbon composites can be made from the modified pitch as matrix precursor by constant-pressure soaking and carbonization technology. This process can simplify the carbon/carbon composite technology, lower the production cost, and promote the composite properties.

II. Analysis of Property Modification Mechanism

In view of the special composition and structure of coal tar pitch, one of the conditions to select the crosslinking catalyst is that it can supply a methylene, so that the thermal chemical reaction will connect the arenes of the

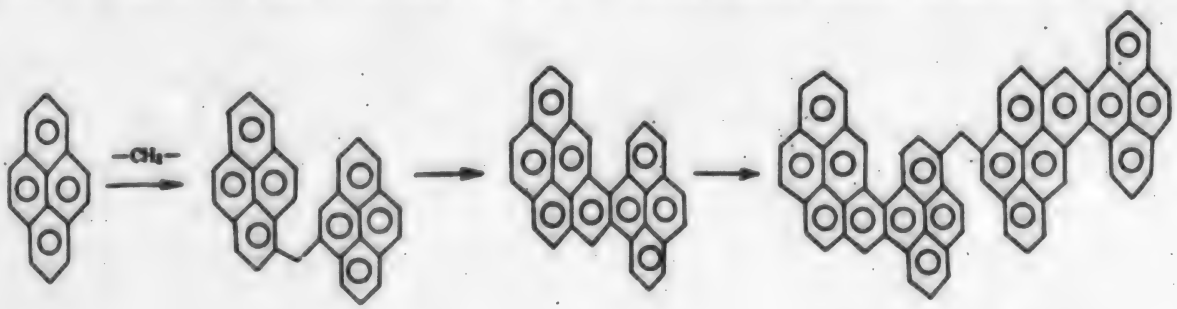

low molecules into a large planar network and form a large molecular structure, thus increasing the C/H ratio in each molecule. The result will be further improved when a benzene ring is also added. Based on this principle, the following reagents are considered as good candidates: p-phenyl dicarbinol, p-phenyl dichloromethane, para-toluenesulfonic acid, trioxymethylene, and formaldehyde monomer. However, some of the candidate catalysts are difficult to synthesize; some, toxic; and some, unstable. The relatively ideal crosslinking catalysts are formaldehyde monomer and para-toluenesulfonic acid. For example, the crosslinking process of pyrene is shown in the following diagram.

III. Experiment and Results

The industrial mesothermal pitch (softening temperature, 82°C; average molecular weight, 460) produced by Wuzhu Steel Company is used for this experiment. The test agents are commercially pure chemical reagents. The experimental process is as follows: The pitch is first pulverized. It is mixed in the crosslink catalyst and uniformly dissolved in a solvent. This is done under the protection of argon where the solution is heated in an oil bath to a pre-set temperature and then cooled rapidly. Both the modified pitch and the unmodified pitch are used as matrix precursors. They are soaked, then carbonized to make two different carbon/carbon composites. Both composites are tested for C/H values, carbon yield rates, softening points (using the ring ball method), and initial temperatures for weight loss (using the thermal gravimetric method), as well as their room-temperature strengths (25°C, 90° direction) and high-temperature strengths (900°C, 90° direction, in air).[3] Table 1 shows the test results.

Table 1. Pitch Properties, Before and After Modifications

	C/H (atomic ratio)	Residue carbon (%)	Softening point (°C)	Temperature at start of weight loss (°C)	Carbon/carbon composite compressive strength	
					Room temperature (MPa)	High temperature (MPa)
Before modification	1.62	50.0	82	220	95	82
After modification	2.01	85.5	108	302	200	191
Increased rate (%)	24.1	71.0	31.7	37.3	110.5	132.9

Note: All values are averaged values.

The crosslinking reaction increases the C/H value of each molecule which leads to an increase in carbon yield rate, and eventually raises the material integrity, lowers its porosity, and betters its heat resistance. Consequently, both the room-temperature and high-temperature strengths of the carbon/carbon composite are promoted.

IV. Conclusions

In China, this experiment is the first using the crosslinking catalyst method to modify domestic industrial coal tar pitch for use as the matrix precursor of an actually fabricated carbon/carbon composite. Based on the experimental results, research on the improvement of pitch properties promises bright potential in industrial application.

References

1. Otani, Sugio, "Thermal Behaviors of Copra Resins From Anthracene and Phenanthrene as Raw Materials," TANSO, 1988, (132): 9-14.
2. Demidova, A. I., COKE CHEM., 1990, (1):53.
3. Li Tiehu, "Matrix for C/C Composites—The Synthesis and Properties of COTAP," Proceedings of Seventh National Conference on Composite Materials (Vol 1), D-18, 1992, 6 [in Chinese].

Synthesis and Application of Hepatitis C Virus Peptides C_1, C_2, and N_1, N_2

40091004A Shanghai ZHONGHUA CHUANRANBING ZAZHI [CHINESE JOURNAL OF INFECTIOUS DISEASES] in Chinese Vol 11 No 3, Aug 93 pp 125-129

[English abstract of article by Lu Zhimeng [7120 1807 2916, Zhang Yan [1728 5333], et al., Ruijin Hospital, Shanghai Second Medical University]

[Text] Three different peptides derived from immunodominant regions of both core and nonstructural proteins based on recognized HCV genome sequences were designed, and a sensitive and specific enzyme-linked immunosorbent assay using these peptides (C_1, C_2, N_1, N_2) as the coated antigen was developed. The specificity of antibodies to these peptides was evaluated by inhibition test and the ranges of inhibition rate was 77% to 100%. We detected 44 serum samples and the results obtained were in agreement with the Abbott 2nd-Generation Kit in 97.7% of the samples. 1,025 samples from various clinical groups were tested for anti-HCV and the antibodies were detected in 43.9% of chronic NANBH patients, 34.4% of blood dialysis patients, 25% of patients with liver cirrhosis, 17.4% of acute NANBH patients, 16.7% of patients with hepatocellular carcinoma and 2.4%-5.4% of volunteer blood donors. The result showed that this assay is of fairly good value in clinical practice.

Investigation of Specific Circulating Immune Complex in Patients With Dengue Fever

40091004B Shanghai ZHONGHUA CHUANRANBING ZAZHI [CHINESE JOURNAL OF INFECTIOUS DISEASES] in Chinese Vol 11 No 3, Aug 93 pp 146-149

[English abstract of article by Shi Shuxian [4258 3219 0103], Song Peihui [1345 0160 6540], et al., Tongji Hospital, Tongji Medical University, Wuhan]

[Text] In order to study the pathogenesis of dengue fever the sodium dodecyl sulfonate polyacrylamide gel electrophoresis (SDS-PAGE) and Western blot techniques were employed to investigate the sera circulating immune complex (CIC) in 28 patients with dengue fever (DF). Three bands of 20 Ku, 46 Ku and 57 Ku were detected in the gels of SDS- PAGE, The existence of specific virus antigens, IgG, IgA, IgM and C_3 in CIC was demonstrated by immunologic recognition.

Establishment and Verification of Animal Model of Immunological Tolerance Against Hepatitis B Virus

40091004C Shanghai SHANGHAI YIKE DAXUE XUEBAO [ACTA ACADEMIAE MEDICINAE SHANGHAI] in Chinese Vol 20 No 5, Sep 93 pp 321-326

[English abstract of article by Xiong Sidong [3574 1835 2639], Zhang Wei [1728 4850], et al., Laboratory of Molecular Virology, Shanghai Medical University, Shanghai]

[Text] In order to establish an animal model of immunological tolerance against Hepatitis B Virus (HBV), one-day old newly hatched ducklings were experimentally infected by injection of duck hepatitis B virus (DHBV) positive serum simulating perinatal transmission of HBV. Both DHBs/presAg and DHBV DNA remained positive at 22 weeks follow-up. ELISA detected neither DHBs/pres antibody nor DHBc antibody in sera Viral DHBs/presAg and DHBcAg antigen specific lymphocyte proliferation of DPBLs were also not observed. For further verification, purified DHBs/presAg and DHBcAg were used to immunize the persistently infected ducks. Antibodies and lymphoproliferative responses to DHBs/presAg and DHBcAg were not detected. Thus, an animal model of immunological tolerance induced by DHBV infection in one-day old ducklings was well established and verified. These results may have implications for the study of immunological tolerance against HBV and future therapeutic strategies.

Effect of Recombinant Interleukin-6-Pseudo-Monas Exotoxin Chimeric Protein (IL-6-PE40) on In Vitro Granulopoiesis of Normal BN Rat

40091004D Beijing ZHONGGUO YINGYONG SHENGLIXUE ZAZHI [CHINESE JOURNAL OF APPLIED PHYSIOLOGY] in Chinese Vol 9 No 3, Sep 93 pp 241-245

[English abstract of article by Xi Yongzhi [1153 3057 1807] and Tang Peixian [0781 0160 1720], Department of Hematopoiesis, Institute of Basic Medical Sciences, Beijing; Anton C.M. Martens and Anton Hagenbeek, Department of Hematology-Oncology, Institute of Applied Radiobiology and Immunology, TNO, NL; and David J. FitzGerald, Laboratory of Molecular Biology, National Cancer Institute, U.S.]

[Text] The fusion protein of IL-6-PE40 which is composed of human interleukin 6 fused with mutant form of pseudomonas exotoxin (PE) devoid of its native cell recognition domain can kill tumor cells expressing high levels of IL-6 receptors. In the present study, cytotoxic effect of IL-6-PE40 on granulopoiesis of bone marrow in normal BN rate was assessed and compared with effect of human IL-6 using granulocyte- macrophage colony forming unit (CFU-GM) and ^{3}H-TdR incorporation assays. The fused protein of IL-6-PE40 is cytotoxic to U266, a human myeloma cell line expressing high levels of IL-6 receptors on the cell surface. The dose of IL-6-PE40 required to inhibit protein synthesis by 50% was 10ng/ml, while 1,000ng/ml of IL-6-PE40 produced 100% inhibition of protein synthesis. In contrast, there was no obvious cytotoxic effect on CFU-GM growth and DNA synthesis in normal bone marrow at the dose range of 1-1,000ng/ml of IL-6-PE40. On the other hand, rhIL-6 itself at a dose range of 1,000U/ml to 4,000U/ml was able to support moderately CFU-GM growth and DNA synthesis. These findings provide evidence that granulocyte-macrophage hematopoietic progenitors and bone

marrow cells do not express IL-6 receptors on their surface and are not sensitive to IL-6-PE40 in vitro.

Studies of Purification, Inactivity and Immunogenicity of Antigenically Chimeric Poliovirus

40091004E Beijing ZHONGGUO YIXUE KEXUEYUAN XUEBAO [ACTA ACADEMIAE MEDICINAE SINICAE] in Chinese
Vol 15 No 5, Oct 93 pp 349-353

[English abstract of article by Cai Hongrong [5591 1347 2837] and Dai Changbai [2071 7022 2672], Institute of Medical Biology, Chinese Academy of Medical Sciences, Kunming]

[Text] Purified polio viruses were inactivated with 1:4000 formalin at 37°C for 12 days. Before and after inactivation, XF414 with anti- PV-1 and anti-PV-2, XF_3 with anti-PV-1 and anti-PV-3 were observed by immunoelectron microscopy and the results were positive.

Neutralization inhibition test and D-Ag unit detection were conducted, and the results were as follow: XF414 had type 1 D-Ag 15971 units/ml and type 2 D-Ag 15644 units/ml; XF_3 had type 1 D-Ag 13314 units/ml and type 3 D-Ag 15971 units/ml. When rabbits were immunized with XF414 and XF_3, they produced bivalent antiserum; i.e., anti-PV-1 and anti-PV-2 induced by XF414 and anti-PV-1 and anti-PV-3 induced by XF_3.

The Cloning and Complete Sequencing of Human Nuclear Protein P68 cDNA

40091006A Beijing BEIJING DAXUE XUEBAO [ACTA SCIENTIARUM NATURALIUM UNIVERSITATIS PEKINENSIS] in Chinese
Vol 29 No 6, Nov 93 pp 655-659

[English abstract of article by Hu Meihao [5170 5019 3185] of the Department of Biology, Peking University]

[Text] The cDNA encoding human p68 protein has been isolated from a cDNA library prepared from human placenta cells. Four mixed oligonucleotides have been synthesized for hybridization. These oligonucleotides have been deduced from the p68 amino acids sequence. Characterized by chain termination sequencing method, the cDNA consists of 2287 nucleotides and shows an open reading frame encoding a polypeptide of 614 amino acids. The cDNA may cover the 5' non-coding region of the p68 mRNA and a 3' non-coding region. In comparison with a recently published p68 cDNA sequence, there is 100 percent homology within the coding region and the 3' non-coding region obtained by this laboratory is more complete.

Key words: P68 protein; λgt11 cDNA library; DNA sequencing

Secondary Structure Study of Huwentoxin-I, a Neurotoxin From the Venom of the Spider Selenocosmia Huwena

40091006B Beijing BEIJING DAXUE XUEBAO [ACTA SCIENTIARUM NATURALIUM UNIVERSITATIS PEKINENSIS] in Chinese
Vol 29 No 6, Nov 93 pp 668-674

[English abstract of article by Liang Songping [2733 1345 1627] and Zong Xiang [4912 3276] of the Department of Biology, Hunan Normal University, and Luo Jingchu [5012 7234 0443], Jing Hua [2417 5478], et al. of the Department of Biology, Peking University]

[Text] Selenocosmia huwena was recently identified as a new species of bird spider of genus Selenocosmia. It is distributed in the high area of Yunnan and Guangxi in the south of China. This spider is rather aggressive and venomous. By means of reverse phase and ion-exchange high performance liquid chromatography, a low molecular weight peptide neurotoxin named huwentoxin-I (HWTX-I) was purified from the venom of the spider Selenocosmia huwena. This toxin can cause paralysis and rapid respiratory failure in mice. The intraperitoneal and intracisternal LD_{50} of HWTX-I in mice were 0.7 mg/kg and 9.4 μg/kg respectively. Electrophysiological experiments indicated that it can block the neuromuscular transmission of the isolated mouse phrenic nerve-diaphragm preparation.

This toxin consists of 33 amino acid residues with three disulphide bonds. The circular dichroism spectra of the toxin in different conditions were measured and analyzed. The contents of various secondary structure elements were calculated with the computer program according to the method of Greenfield. 22-28 percent of amino acid residues is in α-helix, 22-35 percent in β-sheet and 41-49 percent in random coil or β turn. The contents of secondary structure elements of the toxin were found to be relatively stable under different pH and after heating at 80°C for 20 min. The investigation with different methods of secondary structure prediction reveals that most part at the middle of the peptide sequence of the toxin is in random coil or β-turn conformation, while a small β-sheet is formed at the N-terminal and an α-helix at the C-terminal.

Cloning of Human Granulocyte Colony-Stimulating Factor cDNA and Its Expression in Escherichia Coli

40091006C Beijing BEIJING DAXUE XUEBAO [ACTA SCIENTIARUM NATURALIUM UNIVERSITATIS PEKINENSIS] in Chinese
Vol 29 No 6, Nov 93 pp 675-679

[English abstract of article by Zhu Shenggeng [2612 5110 1649], Xiao Zhizhuang [5135 1807 1104], et al. of the Department of Biology, Peking University, and Qin Shulin [4440 2885 2651], Wang Aixia [3769 1947 7209], et al. of the Department of Internal Medicine, Peking Union Hospital]

[Text] Monocytes were isolated from freshly prepared peripheral blood of a healthy adult human and were stimulated by lipopolysaccharide (LPS) to produce hG-CSF. The hG-CSF appeared in culture after 12 hours induction and to be maximum through 24 hours. The total RNA were isolated from human monocytes induced by LPS by using the method of acid guanidinium-phenol-chloroform extraction and amplified specifically by reverse transcription (RT-PCR) technique to obtain hG-CSF cDNA. The optimal annealing temperature determined experimentally was 57°C, at which the reaction product for hG-GSF cDNA was maximized and non-specific products were reduced. The hG-CSF cDNA was inserted into the secretion expression vector pIN-ompA reformed by the laboratory, and then transformed competent E. coli. Recombinant plasmids were identified by restriction enzyme assay and Southern hybridization with 3' terminal, 5' terminal and middle sequence probes. After induction using IPTG, the hG-CSF protein was detected in the periplasmic space of the recombinant E. coli cells. These data provide evidence that hG-CSF cDNA has been cloned and expressed in E. coli.

Key words: hG-CSF; cDNA cloning; Secretion expression vector

Cloning and Expression of H:man CD4 Gene in E. Coli

40091006D Beijing ZHONGHUA WEISHENGWUXUE HE MIANYIXUE ZAZHI [CHINESE JOURNAL OF MICROBIOLOGY AND IMMUNOLOGY] in Chinese Vol 13 No 5, Oct 93 pp 281-284

[English abstract of article by Ji Changhua [0679 2490 5478], Su Chengzhi [5685 2052 5347], et al. of the Department of Biochemistry, The Fourth Military Medical University, Xi'an]

[Text] CD4 molecule is an important differentiation antigen of T lymphocyte and has been identified as the receptor for HIV. We have designed and chemically synthesized two primers, and successfully amplified a gene fragment encoding the N-terminal two domains of human CD4 protein. EcoRI and Hind III recognition sites and the initiation and termination codons were incorporated into the 5' and 3' termini of this gene through polymerase chain reaction. The CD4 gene fragment was digested with EcoRI and Hind III and inserted into pUC19 plasmid. The recombinant clones were confirmed by polymerase chain reaction and restriction endonuclease cleavages and one of the correct clone pT403 was sequenced by dideoxynucleotide termination method and it revealed that the sequence of the cloned gene fragment was identical to that of the published CD4 cDNA. The CD4 gene was then inserted into the prokaryotic expression plasmid pSM43 and transformed TAP106 bacteria, through induction at 42°C, a new protein band appeared in the recombinant bacteria as seen on SDS-PAGE gels. The expression reached its highest level at 5 hours' induction when the CD4 protein accounted for 24.8 percent of the total bacterial proteins. By a few steps of purification, the CD4 protein was shown as a single band on SDS-PAGE.

Expression of Human Recombinant Interleukin-1 Receptor Antagonist (rhIL-1ra) in E. Coli With High Efficiency

40091006E Beijing ZHONGHUA WEISHENGWUXUE HE MIANYIXUE ZAZHI [CHINESE JOURNAL OF MICROBIOLOGY AND IMMUNOLOGY] in Chinese Vol 13 No 5, Oct 93 pp 285-287

[English abstract of article by Di Chunhui [3695 2504 6540], Ma Dalong [7456 1129 7893], et al. of the Department of Immunology, Beijing Medical University]

[Text] The cDNA coding for mature protein sequence of human interleukin-1 receptor antagonist (IL-1ra) was amplified from a lectin activated human peripheral mononuclear cell cDNA library with PCR technique. The purified PCR products were subcloned into an expression plasmid vector pKpL-3a and a clone expressing human recombinant IL-1ra with high efficiency was obtained. The N-terminal amino acid analysis determined that the recombinant protein had a sequence "MRPSGRKSSK", which was identical with the predicted rhIL-1ra sequence. The expressed rhIL-1ra represented about 30 percent of the total bacterial proteins as shown by SDS-PAGE analysis. Biological assay in vitro showed that the rhIL-1ra inhibited the stimulatory activity for thymus cells of monocyte-derived IL-1.

Study on Invasive Ability of the Avirulent Recombinant S. Typhimurium Expressing E. Coli LT-B Antigen

40091006F Beijing ZHONGHUA WEISHENGWUXUE HE MIANYIXUE ZAZHI [CHINESE JOURNAL OF MICROBIOLOGY AND IMMUNOLOGY] in Chinese Vol 13 No 5, Oct 93 pp 305-308

[English abstract of article by Zhang Beining [1728 5563 1337], Yang Xiao [2799 2556], et al. of the Institute of Biotechnology, Academy of Military Medical Sciences]

[Text] The lab had reported that avirulent *S. typhimurium* Δcya Δcrp Δasd strains used as the host could express *E. coli* LT-B sub-unit stably. The recombinant strain had good safety, antigencity and efficient protection. The strain's invasive ability, which might be associated with the immunological mechanism, is being studied here.

The adhesion and penetration of the recombinant strain were observed using HeLa cells. It was found that 50 percent of HeLa cells was infected with the recombinant strain. Counting the number of bacteria showed that 10.53 percent of live bacteria invaded into cells, and propagated in 1 hour. The live bacteria could propagate 6.1-fold in 4 hours.

BALB/c mice were fed orally with the recombinant strain and the bacteria from various organs were isolated every day. The results proved that the recombinant strain could invade mesenterium lymphoid tissue and spleen of the mice, but not heart and liver. The recombinant strain could colonize and propagate in the mesenterium lymphoid tissue, the quantity of bacteria reached the peak in 5th day after infection, and then reduced. The control *E. coli* strain had no invasion to the tissues of mice.

Key words: ETEC [Enterotoxin E. coli]; Heat-labile toxin; Avirulent S. typhimurium; Invasive ability; Immunological mechanism

Genotypic Identification of *Rickettsia Conorii* Seven Strains Using PCR/RFLP Analysis

40091006G Beijing ZHONGHUA WEISHENGWUXUE HE MIANYIXUE ZAZHI [CHINESE JOURNAL OF MICROBIOLOGY AND IMMUNOLOGY] in Chinese
Vol 13 No 5, Oct 93 pp 313-315

[English abstract of article by Zhang Xiaofeng [1728 2556 1496], Fan Mingyuan [5400 2494 6678], et al. of the Department of Rickettsiology, Institute of Epidemiology and Microbiology, Chinese Academy of Preventive Medicine, Beijing]

[Text] Restriction-endonuclease fragment length polymorphism analysis (RFLP) of polymerase chain reaction (PCR) amplified DNA was used to characterize the genotypic diversity of seven strains of *Rickettsia conorii* from south Africa, Ethiopia, Morocco, India and Russia. The strains of *R. conorii* were divided into four genotypes by the RsaI and PstI endonuclease digestion of PCR amplified rickettsial DNA derived from the *Rickettsia rickettsii* 190 kD antigen gene primers. M-1 and Barbash strains, Ethiopian, Indian and S_7 strains were genotypically identical respectively. Simko and Moroccan strains were genotypically different from each other and other strains of *R. conorii*. We concluded that the genotypic diversity existed in intraspecies of *R. conorii*.

Key words: *Rickettsia conorii*; Genotypic identification; PCR/RFLP

Amplification and Cloning of Hog Cholera Virus cDNA Fragments

40091006H Beijing GAOJISHU TONGXUN [HIGH TECHNOLOGY LETTERS] in Chinese Vol 3 No 10, Oct 93 pp 27-30

[English abstract of article by Li Hongwei [2621 4767 5898], Tu Changchun [3205 7022 2504], et al. of the Veterinary Institute, University of Agriculture and Animal Sciences of PLA, Changchun]

[Text] According to the nucleotide sequence of genome of HCV Alfort strain 8 primers were designed and chemically synthesized, and by reverse transcription-polymerase chain reaction (RT-PCR), 5 cDNA fragments of the Chinese shimen HCV strain were amplified from total RNA extracted from HCV infected PK15 cells. Agarose gelelectrophoresis of RT-PCR products indicated that their sizes correspond to the expected 693bp, 346bp, 285bp and 120bp. Endonuclease digestion assay of the amplified fragment PI/PA4 confirmed the results. Two of them with the sizes of 346bp and 120bp were cloned into pUC19 vectors.

A PCR Procedure for the Preparation and Labeling of DNA Inserts Cloned in pUC Plasmid

40091006I Beijing GAOJISHU TONGXUN [HIGH TECHNOLOGY LETTERS] in Chinese
Vol 3 No 11, Nov 93 pp 35-37

[English abstract of article by Yang Zhongwei [2799 1813 0251], Lin Yunfu [2651 0061 1381], et al. of the Institute of Genetics, Fudan University, Shanghai 200433]

[Text] A pair of PCR primers were selected from the sequence flanking cloning site of pUC18, and a universal PCR procedure was constructed for the preparation and radiolabelling of DNA inserts cloned in pUC plasmid. This PCR procedure facilitated the identification of insert DNA length as well as preparation of inserts. The effectiveness of radiolabelling by PCR was identified through Southern blotting of some human X chromosome specific single copy probes.

Isolation of Venom of Naja Naja atra and Its Toxicity Determination in Different Fractions

40091006J Nanning SHE ZHI [JOURNAL OF SNAKE] in Chinese Vol 5 No 3, Sep 93 pp 6-8

[English abstract of article by Cao Yisheng [2580 1355 3932] and Liu Zhiping [0491 1807 1627] of the Guangzhou Military Medical Institute, Guangzhou]

[Text] The venom of Naja naja atra (from Hunan) was fractionated on CM-cellulose into 15 different fractions, among which were four neurotoxic components. When the two main fractions were collected, they produced a sc LD50 of 0.13 mg/kg, nearly nine and two times, respectively, more toxic than the unfractionated venom and KTL (neurotoxin purified in Guangxi). The result on polyacrylamide gel electrophoresis demonstrated that the protein migration rates of the four neurotoxic components were 0.64, 0.70, 0.76 and 0.82. Three protein bands were identified in KTL, whereas more than 10 bands were indicated in unfractionated venom.

Key words: Venom, Neurotoxin, Bioactivity, Isolation fractionation.

Clinical Research of Sudden Deafness Treated With Pallas Pit Viper Antithrombase

4009100oX Nanning SHE ZHI [JOURNAL OF SNAKE] in Chinese Vol 5 No 3, Sep 93 pp 26-28, 16

[English abstract of article by Zhang Heping [1728 0735 1627], He Guangxiang [6320 1639 3276], et al. of the Central Hospital of Shouyang City, Hunan]

[Text] Eighty cases of sudden deafness have been treated by our hospital from March 1991 to November 1992. All cases were divided into treatment group and control group at random. Among 44 ears, 40 cases of the treatment group were treated by pallas pit viper antithrombase. The recovery rate is 47.7 percent and the efficient rate 81.8 percent. Among 48 ears, 40 cases in control group were treated by Dextraumn-40.654-3. salvia miltiorrhiza, virazole etc. The recovery and efficiency in the treatment group is markedly higher than that of the control one ($P < 0.05$, $P < 0.01$). Erythrocyte sedimentation rate (ESR) and fibrinogen in the treatment group drops markedly after treatment, but the control group doesn't. The result of the research shows that the therapeutic efficiency of the antithrombase to sudden deafness is notable and its side effect is little. It is believed that use of snake venom products provides a new way to treat sudden deafness.

Effects of Two Kinds of Chinese Herb Medicine on Rabbit's Ear Microcirculation Under Simulated Weightlessness

40091005A Beijing HANGTIAN YIXUE YU YIXUE GONGCHENG [SPACE MEDICINE & MEDICAL ENGINEERING] in Chinese Vol 6 No 1, 1993 pp 1-5

[English abstract of article by Shen Xianyun [3088 5029 0061], Xiang Qiulu [0686 3061 7627], and Meng Jingrui [1322 0079 3843] of the Institute of Space Medico-Engineering, Beijing]

[Text] A study has found that the overall picture of the circulatory changes during weightlessness (WL) or simulated weightlessness (SWL) well resemble that of "blood stasis" as named in Chinese medicine. So the researchers suggested that certain kinds of Chinese herb medicine may be effective in improving the functional state of blood circulation under WL or SWL. In this experiment, the effects of two kinds of Chinese herb medicine, Chuan Qiong (CQ) and Dan Sun + Huang Qi (DH) on rabbit's ear microcirculation under SWL were observed. Changes of ear microcirculation in four groups of rabbits (moving freely + water group, head down tilt + water group, head down tilt + CQ group and head down tilt + DH group) before and after SWL for 6 days were observed. The results indicated that CQ and DH had effects of improving the conditions of ear microcirculation in SWL rabbits, and the effect of DH seemed to be better than that of CQ. So Chinese herb medicine may have a good prospect of being used in space flight.

Key words: weightlessness simulation, countermeasure, Chinese traditional and herbal drugs, microcirculation.

Protection of Chinese Medicine and Low Frequency Magnetic Field Against Suspension Induced Bone Loss in Rat

40091005B Beijing HANGTIAN YIXUE YU YIXUE GONGCHENG [SPACE MEDICINE & MEDICAL ENGINEERING] in Chinese Vol 6 No 1, 1993 pp 12-18

[English abstract of article by Shi Zhizhen [0670 0037 4394], Shen Shiliang [3088 1102 5328], and Cui Wei [1508 0251] of the Institute of Space Medico-Engineering, Beijing]

[Text] The protective effects of Chinese medicine and extremely low frequency magnetic field stimulation (LMF) on bone loss were studied in 100 S. D. male rats during 21-day tail suspension. The main results were: as compared with suspension control group, bone formation rate of tibia, mechanical strength of femura, mean density of mineral contents of weight-bearing bone and calcium contents in serum were all increased by Chinese medicine or LMF. In addition, the condition of periosteum was significantly improved by LMF. The results also indicated that collaboration exists between Chinese medicine and LMF, thus much better protection against suspension induced bone loss could be obtained by the use of both means.

Key words: weightlessness simulation, bone loss, Chinese traditional and herbal drugs, low frequency magnetic field, countermeasures.

Radiation Dose Measurement and Biostack Experiment in Biocabin on Board Satellite

40091005C Beijing HANGTIAN YIXUE YU YIXUE GONGCHENG [SPACE MEDICINE & MEDICAL ENGINEERING] in Chinese Vol 6 No 1, 1993 pp 19-23

[English abstract of article by Chen Mei [7115 3270], Qi Zhangnian [4359 4545 1628], and Li Xianggao [2621 0686 7559] of the Institute of Space Medico-Engineering, Beijing, and Zhuang Dahuan [8369 1129 2719] of the Institute of Sericulture, Zhenjiang]

[Text] Radiation doses outside and inside the biocabin on board the Chinese recoverable satellite were measured with LiF thermoluminescent dosimeters. The dose level was 0.53 +/- 0.04 mGy accumulated in 8 day flight period, which corresponds to 0.07 mGy/d, and is about 28 times as high as the ground control value. A kind of biostack, sandwiched silkworm eggs and CR-39 plastic nuclear track detectors, was designed for recording the high atomic number and high energy (HZE) particles from the cosmic ray and their biological effect.

Evaluation of Speech Technology for Enhancing Performance of Man-Machine Systems

40091005D Beijing HANGTIAN YIXUE YU YIXUE GONGCHENG [SPACE MEDICINE & MEDICAL ENGINEERING] in Chinese Vol 6 No 1, 1993 pp 31-38

[English abstract of article by Chen Shanguang [7115 0810 1639] and Jiang Qiyuan [3068 3217 6678] of the Institute of Space Medico-Engineering, Beijing]

[Text] In this study, effects of speech input and output technology on performance of man-machine systems were evaluated through four types of target tracking tasks denoted as SK, CK, SS and CS where the first letter /S/ or /C/ represented the display modes in speech or character on CRT screen for informing the directions of tracking, and the second letter /S/ or /K/ referred to data input mode using speech or keyboard respectively. It was shown that the mean ORT (Operation/Response Time) for Task SK was 6.3 percent less than that for Task CK, the mean ORT for Task SS was 5.8 percent less than that for Task CS. Among the mean ORTs for all the four types of tasks, ORT for Task SS was the shortest, while that for Task CK was the longest. The ORER (Operation/Response Error Rate) of speech display mode (2.75 percent) was much lower than that of CRT display mode (5.38 percent), however, the ORER of speech input mode (2.98 percent) was higher than that of keyboard input mode (1.13 percent). This might be resulted from limited performance of the speech recognition system and the speech variations of individual subjects. These results imply that people are more natural to perceive speech information than screen-displayed messages and can also react more quickly and correctly to speech cues, and if speech input modality is adopted appropriately in multiple-task situation, operator's workload can be reduced and system performance can be improved. In conclusion, speech technology is feasible for enhancing man-machine system performance. However, adequate considerations should be made in terms of the interactions among such factors as human operator, machine, environment and task demands.

Human Head-Neck Tolerance to Windblast

40091005E Beijing HANGTIAN YIXUE YU YIXUE GONGCHENG [SPACE MEDICINE & MEDICAL ENGINEERING] in Chinese Vol 6 No 2, 1993 pp 79-87

[English abstract of article by Zhang Yunran [1728 0061 3544], Wu Guirong [0702 2710 2837], et al. of the Institute of Space Medico-Engineering, Beijing]

[Text] Up to now, a major threat against aircrewman life is still due to windblast and ejection seat instability during high-speed ejection. The purpose of this paper is to obtain the human head-neck region tolerance to windblast. Wind tunnel tests of human head and neck region of a 1/10 scale model crewman and ejection seat at transonic-supersonic speed were conducted to determine aerodynamic force exerted on head and neck region by windblast. Change of aerodynamic force v.s. time during ejection sequence was calculated and diagrammed. Simulation tests were made in monkey's head-neck region with a dynamic load simulator according to the data obtained from wind tunnel tests. Monkey tolerance to simulated aerodynamic effect was obtained by vivisection physiological-biochemical and biodynamic measures. After that, the data were compared with the results of investigations and studies on aviation accident and human biodynamic tolerance. It is suggested that human head-neck tolerance to windblast could be set at 1000 km/h.

Experimental Studies on Head Neck Muscle Trauma in Rhesus Monkeys

40091005F Beijing HANGTIAN YIXUE YU YIXUE GONGCHENG [SPACE MEDICINE & MEDICAL ENGINEERING] in Chinese Vol 6 No 2, 1993 pp 88-94

[English abstract of article by Wang Yijin [3769 0110 6651], Li Wei [2621 0251], et al. of Shanghai University of Science and Technology, Shanghai, and Wu Guirong [0702 2710 2837], Zhang Yunran [1728 0061 3544], et al. of the Institute of Space Medico-Engineering, Beijing]

[Text] The design of protective equipment for the head is often based on intuition because of the lack of reliable information about the mechanical behavior of the head. In order to properly design devices for minimizing head injury in the projective crash environment, engineers require a means for predicting the potential injury model. The objective of this study was to perform experiments on head of animals and fresh cadavers with sufficient precision so that a validation of the analytical model can be made for the impact situation, and to analyze the mechanisms of head injury in animal tests with pathological and engineering data obtained from the experiments. The neck is susceptible to trauma and is frequently a site of pain. Thus, determination of the magnitudes of neck muscle impact forces and of cervical spine compression and shear forces imposed by the performance of physical tasks are of practical importance. A series of experimental results related to the biomechanical properties for four cases of severe head neck muscle injury in rhesus monkeys were presented. It includes muscle contraction intensity, forces and strain, rotation acceleration and so on. A biomechanical model of the neck muscle was constructed. It was found that the primary types of strain that damage tissue were tensile strain and shear strain, which produce lacerations, fractures, ruptures or avulsions. When an artery is stretched beyond its tensile strength, the tissue will break. Organs and vessels were stretched in different ways, which result in different types of injuries. Shear strain occurred when opposing forces acted across a tissue. The strain mechanism not only explains laceration injuries but was also a principal factor in contusion injury. The present results would be helpful in the treatment of injury of the head-neck region and design of its protective equipments.

A Study of Endurance Limit of Monkey's Head-Neck Region to Simulated Aerodynamic Loads

40091005G Beijing HANGTIAN YIXUE YU YIXUE GONGCHENG [SPACE MEDICINE & MEDICAL ENGINEERING] in Chinese Vol 6 No 2, 1993 pp 95-99

[English abstract of article by Wu Guirong [0702 2710 2837], Zhang Yunran [1728 0061 3544], et al. of the Institute of Space Medico-Engineering, Beijing]

[Text] Head-neck injuries caused by high-speed windblast is an important problem in emergency ejection. Simulated windblast impact was applied to the head of 24 monkeys by means of a specially designed dynamic loader to simulate the windblast curves acting on human body during emergency ejection. Endurance limit of monkeys head-neck region to simulated aerodynamic loads was evaluated with medical parameters. The experimental results indicated that 2.3 kN impact load caused no injury in monkeys; impact load causing concussion of brain in monkeys was 2.5 kN; at this load obvious congestion in the brain, and hemorrhage in muscles and subcutaneous tissue in the back of neck were observed. Dissolves of Nissl body was found under microscope, but red cell and CK-BB were not found in cerebrospinal fluid (CSF); impact load threatening monkey's life was 2.8 kN and above. Fracture of skull, brain injuries, tear of muscles in the neck and the back may be observed at this load, and red cells and CK-BB were found in CSF. The experimental results could serve as basis for the determination of endurance limit of human head-neck region to windblast. The specially designed dynamic loader used in the experiment was found to be an ideal device in experimental studies on impact injury.

A Preliminary Observation on Changes of Somatostatin Immunoreactive Cells in the Gastric Antrum and Duodenum During Simulated Weightlessness in Rats

40091005H Beijing HANGTIAN YIXUE YU YIXUE GONGCHENG [SPACE MEDICINE & MEDICAL ENGINEERING] in Chinese Vol 6 No 2, 1993 pp 106-110

[English abstract of article by Fu Chunguang [0265 2504 0342], Su Huici [5685 1979 1964], et al. of the Fourth Military Medical University, Xian]

[Text] Weightlessness has been noted to have widespread effects on body functions. Changes of the cardiovascular system, neuro-muscular functions, etc. had been documented. Somatostatin (SS) is one of the important bioactive peptides, which regulates body functions extensively. The majority of SS in the body are produced by SS immunoreactive cells in the gastrointestinal tract which are predominantly distributed in the gastric antrum and duodenum. In order to investigate the effects of weightlessness on the gastrointestinal SS immunoreactive cells, ABC (Avidin-Biotin-Peroxidase Complex) immuno-cytochemical staining method was applied to the sections of gastric antrum and duodenum of both rats exposed to simulated weightlessness and normal rats to demonstrate the SS cells. Sprague-Dawely rats were randomly and equally divided into two groups, one for ground-based simulated weightlessness test and the other as control. The rats in ground-based weightlessness simulation group were suspended head-down (-30°) by the tail with hind limbs bearing no weight for 3 months. Food and water were supplied freely. The control rats were fed with the same food and water in the same room. Gastric antrum and whole duodenum were dissected out from each rat. Tissues were fixed in 4 percent paraformaldehyde for 24 h and then embedded in paraffin routinely. Sections of 5 μm were cut and mounted on gelatine coated slides. Rabbit anti-SS serum (working dilution 1:4000) and ABC kit were used in this study. Hsu's standard ABC immunostaining procedure was adopted. The results revealed that the SS immunoreactive cells in rats exposed to simulated weightlessness were significantly reduced. The relationship between these effects and the endocrine alterations caused/induced by weightlessness was discussed.

Change of Anaerobic Threshold After Arrival at 4370 m Altitude From Sea Level

40091005I Beijing HANGTIAN YIXUE YU YIXUE GONGCHENG [SPACE MEDICINE & MEDICAL ENGINEERING] in Chinese Vol 6 No 2, 1993 pp 111-114

[English abstract of article by Yin Zhaoyun [1438 2507 0061], Zan Junping [2501 0193 1627], et al. of the Institute of Hygiene and Environmental Medicine, Academy of Military Medical Science, Tianjin]

[Text] A study was conducted in 14 young health normal sea level residents on the changes at physical work capacity during sojourn to high altitude. Initial studies of low landers were carried out at Chengdu (approximately sea level). They were taken to an altitude of 4370 m by air and stayed there for 2 weeks. The subjects exercised on bicycle ergometer to volitional fatigue. After 5 min of unloaded cycling, the work rate was increased by 20 W every 3 min until exhaustion. During the exercise test, the subjects expired into a Douglas bag during the final minute of each 3 min duration. The collected expired gas was immediately assessed for ventilatory gas exchange parameters (V_E, VO_2, $V[dot]co_2$, $V[dot]_E/V[dot]o_2$, $V[dot]_E/V[dot]co_2$). The scores of anaerobic threshold were determined by finding the break point of the systematic increase in $V[dot]_E/V[dot]o_2$ during incremental exercise test (AT_{OE}). The results showed that on the 3rd, 5th, 7th and 14th day after arrival at the altitude of 4370 m, the AT_{OE} decreased by 35.6 percent, 32.4 percent, 40.0 percent and 39.6 percent ($p < 0.01$), respectively, in comparison with the value at sea level. They were close to the experimental value of decreased maximal oxygen uptake (34 percent) at same altitude. Moreover, the reduction of AT_{OE} at high altitude tended to be greater in those with a larger initial AT_{OE} than those with a small initial AT_{OE}. It was still 24.5 percent

($p < 0.01$) lower than the sea level value even after 1 year residence at that altitude. These results suggested that after exposure to high altitude, AT_{GE} decreased markedly and would not return to sea level value after short period. In addition, AT_{GE} might be applicable to the evaluation of work capacity at high altitude.

An Observation on Effects of Puerarin in Treatment of Coronary Heart Diseases With Angina Pectoris and Acute Myocardial Infarction

40091005J Beijing HANGTIAN YIXUE YU YIXUE GONGCHENG [SPACE MEDICINE & MEDICAL ENGINEERING] in Chinese
Vol 6 No 2, 1993 pp 115-119

[English abstract of article by Ren Guizhi [0117 2710 5347], Zhang Ningning [1728 1337 1337], et al. of The Affiliated Hospital of Qingdao Medical College, Qingdao]

[Text] In aviation or spaceflight, factors such as low atmospheric pressure and lack of oxygen encountered in the special environment can cause acute exacerbation of coronary heart disease in pilots and astronauts. Therefore there is certain significance in the treatment of coronary heart disease in the field of aerospace medicine.

In this study, the use of puerarin in the treatment of 29 cases of acute myocardial infarction and angina pectoris and 10 cases of chronic myocardial infarction were reported. The results indicated that in the treated group, heart rate and blood pressure as well as the index of oxygen consumption declined significantly as compared with those before the use of the drug ($p < 0.001$). N_{ST} and N_Q ECG showed significant drop ($p < 0.05$ or $P < 0.01$) or even recovered to normal after 3-15 days of treatment.

Application of Variance Analysis and Similarity Priority Ratio in Research of Prophylaxis and Treatment of Visual Evoked Motion Sickness

40091005K Beijing HANGTIAN YIXUE YU YIXUE GONGCHENG [SPACE MEDICINE & MEDICAL ENGINEERING] in Chinese
Vol 6 No 2, 1993 pp 120-125

[English abstract of article by Sun Hongyuan [1327 3163 0337], Yu Yaorong [0205 1031 2837], et al. of the Institute of Space Medico-Engineering, Beijing]

[Text] The purpose of this study is to test with variance analysis whether there is significant difference between physiological and biochemical indices and whether interaction exists between methods and subjects. Optimal method of prophylaxis and treatment of visual evoked motion sickness was selected using Similarity Priority Ratio. Thirteen healthy male volunteers aged 18-24 years participated in the experiment. Their visual and vestibular functions were normal. Auto-control method was used in the experiment. Three experiment groups, namely blank control group, Acupoint Electric Stimulation (AES) group and Acupoint Magnet Application (AMA) group were designed. 17-OHCS, E, NE, skin O_2, skin temperature, frequency and amplitude of electrogastrogram were examined. Physiological and biochemical indices of subjects were tested using variance analysis. Results indicated that there was significant difference between the methods, and interaction existed between the methods and subjects. AMA and AES methods were effective for prophylaxis and treatment of visual evoked motion sickness. However, AMA was better than AES. Optimal method of prophylaxis and treatment of visual evoked motion sickness was selected using Similarity Priority Ratio. AMA method was found to be optimal and easy in operation. There was no side effect and it was non-toxic. Its use might be helpful in further studies of prevention and control of space motion sickness.

Study on Certain Factors Influencing Human Controlling Ability in Two-Degrees-of-Freedom Compensatory Tracking Tasks

40091005L Beijing HANGTIAN YIXUE YU YIXUE GONGCHENG [SPACE MEDICINE & MEDICAL ENGINEERING] in Chinese
Vol 6 No 2, 1993 pp 126-132

[English abstract of article by Cai Shangchun [5591 1424 4783], Long Shengzhao [7893 0581 3564], et al. of the Institute of Space Medico-Engineering, Beijing]

[Text] According to the theory of man-machine system, the control of man doing two-degrees-of-freedom compensatory tracking tasks under simulated conditions based on the degrees of freedom, dynamics of the controlled objects and bandwidths of the command signals were studied. It was aimed at evaluating the performance of dynamic system and providing some valuable evidence for designing and developing man-machine systems.

Eight healthy men with naked eye vision of 5.0 and aged about 20 years, were selected as the controllers. The dynamics of controlled objects (0.5/s, 0.5/s (0.25s + 1), $0.5/s^2$) were chosen by master on a DJM-5 analogue computer. Demonstration and production of input signals, storage and statistical analysis of the data were carried out on a Compaq 386 computer. The manipulations of input signals of three bandwidths (100, 80, 60) were carried on X-axis, Y-axis and XY-axis. The moving target was made to coincide with the fixed target as far as possible in order to produce control signals. X-in, Y-in, X-out, Y-out were sampled by computer with intervals of 180/3545s in a period of 3 minutes. When these manipulated processes were stabilized after 1 min, system performance was evaluated using fuel consumption of the controller and average values of the square roots of system errors. The parameters were designed on an orthogonal test in this experiment.

Some 852 person-time experiments of eight men were performed and the results obtained were as follows:

When single axis was controlled under conditions of the same dynamics and bandwidths, fuel consumption in X-axis was smaller than that in Y-axis, but system error in X-axis was significantly higher than that in Y-axis.

If only degrees of freedom were considered, a negative correlation and system errors could be obtained.

When the three types of dynamics were considered, the order of fuel consumption derived from dynamics 3, dynamics 2 and dynamics 1 was: dynamics 3 > dynamics 2 > dynamics 1.

To some extent, the bandwidths of command signals also affected the system performance. When the manipulation was easy to control, the narrower the bandwidth of command signal, the smaller the system error was; however, when the manipulation was difficult to control, irregular relation between the bandwidth and the system error could be seen. The effect of bandwidth might be counteracted by the psychological condition of the controller.

The order of the effect of different parameters on the difficulty of manipulation was: dynamics of controlled objects > degrees of freedom > bandwidths of command signals.

There were significant individual differences in the controlling ability of men, and the psychological character of individuals showed a noteworthy effect on system performance.

Fuel consumptions and the system errors derived from the signals of larger magnitude were generally higher than those derived from the signals of smaller magnitude of change.

Based on these results, we could conclude that the performance of the man-machine system could be improved through changing the psychological character of individuals, choosing the method and velocity of demonstration and the structure of instrument of manipulation, and training/selecting the controllers.

Finally, the research direction and assumption in the controlling ability of man in the future are pointed out.

Bio-Mechanical Efficiency of Joint-Muscle System

40091005M Beijing HANGTIAN YIXUE YU YIXUE GONGCHENG [SPACE MEDICINE & MEDICAL ENGINEERING] in Chinese
Vol 6 No 3, 1993 pp 157-165

[English abstract of article by Ma Zhijia [7456 3112 1367] of the Institute of Space Medico-Engineering, Beijing, and E. Andersson and A. Thorstensson of the Department of Physiology 3, Karolinska Institute, S-113 337 Lidingovagen 1, Stockholm, Sweden]

[Text] In order to study the man-machine system relation, researchers investigate the bio-mechanical efficiency of joint-muscle systems, the efficiency of the muscle biceps brachii and elbow joint under different conditions were observed. The results obtained showed that the efficiency of the biceps brachii muscle and elbow joint was a complicated function of the elbow angle, the external force level and the movement velocity of the forearm. The highest efficiencies at different force levels during isometric contractions appeared at 45 and 75 degrees of elbow angle and the efficiency at the same elbow angle decreased with increased external force level. The efficiencies were lower for the dynamic contractions than for the static ones at similar elbow angle and force level. The efficiency for dynamic contractions at 20 percent force level decreased with movement velocity of the forearm and the angle of movement range, but it was difficult to distinguish the effects of the force level and movement velocity at high force levels. Several possible physiological and mechanical causes of the observed results were discussed and possible applications of the observed data were recommended.

A Study of Rabbit's Liver Impact Injury and Its Mechanical Parameters

40091005N Beijing HANGTIAN YIXUE YU YIXUE GONGCHENG [SPACE MEDICINE & MEDICAL ENGINEERING] in Chinese
Vol 6 No 3, 1993 pp 173-181

[English abstract of article by Luo Jin [5012 6651], Wang Yulan [3769 3768 5695], et al. of the Institute of Space Medico-Engineering, Beijing]

[Text] Forty-four rabbits were used in this experiment. The rabbits' livers were exposed by surgical operation and impacted directly by an impact bar. Impact acceleration, impact force and the injury level of the liver were observed. The results demonstrated that liver is a viscoelastic material, its injury was related to stress, strain and rate of strain; when liver injury was evaluated, maximum impact displacement, maximum impact force, maximum viscous response and the average impact power must be considered comprehensively. The appropriate use of the parameters in different impact conditions was important; in dynamic impact condition, average impact power can reflect the injury level in the liver's diaphragmatic surface very well. It is a new parameter which can help us in evaluating liver injury comprehensively.

A Simulation Study on External Counter-Pulsation for Heart Failure Patient

40091005O Beijing HANGTIAN YIXUE YU YIXUE GONGCHENG [SPACE MEDICINE & MEDICAL ENGINEERING] in Chinese
Vol 6 No 3, 1993 pp 204-209

[English abstract of article by Bai Jing [4101 0403], Wu Dongsheng [0702 0392 3932], and Zhang Jupeng [1728 5468 7720] of the Department of Electrical Engineering, Tsinghua University, Beijing. The project was supported by the National Natural Science Foundation of China.]

[Text] In this paper, a hemodynamic computer simulation model for heart failure subject has been established and reported. The failing heart was modelled by a multiplying factor to the ventricular elastance. This model can simulate the heart failure to various degrees. Using this model, a computer simulation study of three step sequential external counter-pulsation has been performed to investigate the effects of the control parameter of the device, especially, the delay of the inflation timing of the three parts of the external pulsating trousers and the duration of the pressure plateau of the pulsing balloons. Six physiological parameters were taken as the output parameters of the simulation experiments, namely, stroke volume, the mean systolic aortic pressure, mean diastolic aortic pressure, mean pulmonary arterial pressure, total coronary flow, and the ratio of the mean aortic diastolic pressure to the systolic pressure. The simulation results indicate that the hemodynamic parameters are affected by the control parameters of the device. Among the physiological parameters studied, the ratio of the mean aortic diastolic pressure to the systolic pressure can be taken as a comprehensive indicator of the efficacy of the external counter-pulsation treatment. This ratio will take its maximal value when the control parameters are optimized. This study also indicates that the Q value would not provide a sufficient condition for the optimal control of the external counter-pulsation. The aortic pressure was monitored to avoid early inflation. The results presented in this paper agree well with the clinical data.

Cytochemical Changes in Rectus Femoris in Rats After 90 Days of Tail Suspension

40091005P Beijing HANGTIAN YIXUE YU YIXUE GONGCHENG [SPACE MEDICINE & MEDICAL ENGINEERING] in Chinese
Vol 6 No 3, 1993 pp 210-215

[English abstract of article by Zhang Jinshan [1728 6855 1472], Su Huici [5685 1979 1964], et al. of the Fourth Military Medical University, Xian]

[Text] The purpose of this study was to investigate the alterations in composition, cross-sectional area and cytochemical properties in the rectus femoris muscle fibers of rat after 90 day tail suspension. Sixteen male Sprague-Dawley rats (207 +/- 18g in body weight) were divided into tail suspended group and control group equally. Left rectus femoris were removed and serial cryostat sections were made. Histochemical reactions for lipid, glycogen, succinate dehydrogenase (SDHase) and alkaline phosphatase (ALP) were observed. Muscle fiber types were divided by histochemical reaction of SDHase. Morphometric results using image processing system showed that the cross sectional fiber areas of types I and II A muscle fibers were decreased markedly in suspended rats as compared with those in controls ($P < 0.01$ and $P < 0.05$ respectively). A significant reduction of type I composition ($P < 0.01$) was accompanied by an increase of type II A subgroup ($P < 0.05$). The normal distribution of 15.9 percent of type I fibers in rectus femoris was decreased to 9.1 percent in suspended rats; whereas type II A increased from 26.1 percent to 34.8 percent. Histochemical quantitative results demonstrated that activity of SDHase were decreased ($P < 0.05$), and glycogen, lipid and ALPase were increased ($P < 0.01$, $P < 0.01$ and $P < 0.05$ respectively) in type I fibers after 90 day tail suspension. Lipid in type II B fibers was also increased ($P < 0.05$) in suspended group. We concluded that prolonged ground simulated weightlessness by 90 days of tail suspension in rats led to the changes of proportions of muscle fibers in rectus femoris, and reduction of oxidase activity and accumulation of glycogen and lipid in type I muscle fibers.

First Domestic Advanced Supercomputer Real-Time 3D Image Generation System Developed

94P60080E Beijing RENMIN RIBAO OVERSEAS EDITION in Chinese 15 Dec 93 p 1

[Article by Xu Jingyue [1776 0079 6460]: "China Develops New Supercomputer System That Can Generate Dynamic Three-Dimensional Images: Its Peak Operating Speed Is 300 MOPS"]

[Summary] Beijing, 14 Dec (XINHUA)—The nation's first advanced supercomputer real-time 3D image generation system—the 2100CIG system—has been jointly developed by engineers at the China Aerospace Corporation's Third Academy and Harbin Institute of Technology. The system, with a peak speed of 300 million operations per second (MOPS), can process 80 million pixels or generate 200,000 triangles or generate in real time lifelike dynamic 3D images from a variety of observation points and with up to 16 million varieties of color. This system is targeted for astronaut training, flight training under complex meteorological conditions, flight fault processing, and missile development. It is understood that so far only the United States has mastered this high technology.

Unveiling a Very High-Tech Pen

40100022A Beijing CHINA DAILY in English 22 Dec 93 p 5

[Article by Ke Ji: "Unveiling a Very Hi-Tech Pen"]

[Text] Many people may have swapped their pens for computers, but the computer industry is doing just the opposite—picking up its pen again.

Since its development in the United States two years ago, the pen computer—where the user writes on the computer screen—has become all the rage in the electronic information industry.

Now, the revolution of pen computer technology has arrived in China, as the latest and most advanced portable pen computer using Chinese was announced earlier this month in Beijing. It is based on Chinese talent and American hardware.

The new PenX 386 and 486 involve the latest technologies of AST Research Incorporated and the Institute of Automation of the Chinese Academy of Sciences (IACAS), and SunTendy Electronic Information Research Institute.

"The new pen computer is the combination of three top technologies, which makes it definitely the best of its kind in China," said Huang Zhuqi, AST's sale supervisor in North Asia.

The first technology is AST's: an advanced 2.5-kilogram portable pen computer with a touch-sensitive liquid crystal screen.

A little bigger than a magazine, it is equivalent to a 386 or 486 personal computer.

It has a hard disc memory capacity of 120 MB (in PenX 386) and 200 MB (in PenX 486).

Meanwhile, with an attached soft disc driver, the pen computer can also use three-inch discs.

In its software, the computer uses an advanced Chinese handwriting recognition system developed by the IACAS.

The third technology is Chinese Star, which is a software that creates a Chinese-language platform for all applied software of the Windows system. Developed by SunTendy, the product allows Chinese users to use Western software in Chinese.

Of course, the computer can operate under English language environment, applying a Windows-for-Pen software developed by US-based Microsoft Company.

"Instead of typing commands, PenX users can merely check a selection on the screen with an electronic pen that is connected to the computer with a cord," said John Carson, a marketing manager with AST. "The pen functions like a mouse, but is much easier and convenient."

This pen computer can read handwritten Chinese. "This pen computer has a special significance for Chinese, who have to face a problem in using computers that foreigners never encounter—inputting Chinese characters," said Associate Professor Liu Yingjian of the IACAS.

"With PenX, Chinese can simply write Chinese characters on the screen, and the computer will recognize most of them," he said.

Liu, who is one of the major developers of the Chinese handwriting recognition system, said his system can recognize more than 130,000 Chinese characters, with an accuracy rate of 95 per cent.

"This is the highest accuracy rate achieved in the country," he said.

The wrong characters can be corrected by rewriting. The system won a first prize in the 1992 Natural Sciences Awards organized by the Chinese Academy of Sciences—and is listed as one of the State 863 Hi-tech Research Programmes.

Using Liu's software, PenX can improve its skills. It will get used to a user's style of handwriting, and gradually increase its rate of character recognition.

Computer experts and users in Beijing are showing great interest in the pen computer. Several hundred people attended a seminar for PenX early this month.

Experts estimate that the computer will become a major draw in the computer industry, predicting that by 1996 the demand for pen computers may reach 5 million.

A new computer has been developed that can read Chinese handwriting.

This year, more than 400,000 pen computers are expected to be sold around the world.

"People are talking about pocket computers. However, as long as we still keep the keyboard we will never be able to actually put it in our pocket," Liu said. "The solution is the pen computer because it gives up the keyboard."

PenX retains its keyboard so it can be used as a standard personal computer. However, the hi-tech involved in it means you could throw your keyboard away—and still use your computer effectively.

Major Neural Network Theory, Applications Study Reaps Benefits

94P60091A Beijing ZHONGGUO KEXUE BAO [CHINESE SCIENCE NEWS] in Chinese 10 Dec 93 p 1

[Article by Zhang Yaguang [1728 0068 0342]: "Basic Research Yields Repayment: Widespread Benefits of Neural Network Study"]

[Summary] A Key State Basic Research Topic, "Study of Neural Network Theoretical Models and Methods for Their Applications," has yielded widespread benefits both in terms of international interest and market products developed from the theory. This 3-year, 105-person study, led by [Professors] Guo Aike [6753 1947 0344] and Huang Taiyi [7806 3141 5065] of the CAS Institute of Biophysics and CAS Institute of Automation, has resulted in such achievements as an 8000-neural-element character-recognition system that can recognize frequently used handwritten Chinese characters: the world's first character-recognition system incorporating large-scale use of nonlinear dynamic network interconnections. Based on this laboratory achievement, engineers in the study quickly developed and marketed the Hanwang [3352 3769] 99 Automatic Chinese-Character Recognition System. Other major achievements include development of a true industrial robot with real-time movement guided by a neural-network-based position controller and development of a neural network target-recognition system that in real time can detect motion of the target image relative to the background. The latter system's control resolution exceeds the international state-of-the-art for such products. Finally, project researchers have designed an optimized modified BP [backpropagation] algorithm with which they developed a neural accelerator card.

Integrated Printed-Chinese-Character Recognition System Certified

94P60080C Beijing KEJI RIBAO [SCIENCE AND TECHNOLOGY DAILY] in Chinese 29 Nov 93 p 1

[Article by Han Yuqi [7281 3768 3824]: "Integrated Printed-Chinese-Character Recognition System Developed"]

[Summary] The [model N1.OCR] integrated printed-Chinese-character recognition system developed by engineers at the State Intelligent Computer R&D Center in collaboration with colleagues at the Beijing Institute of Information Engineering, the CAS Shenyang Institute of Automation, and Qinghua University, on 25 November in Beijing passed the formal appraisal organized by the SSTC's High-Tech Department. This major new optical character recognition (OCR) system, developed under an 863 Plan grant, was strictly tested with over a million characters in texts of varying quality. Overall recognition

accuracy measured over 98 percent, while the misprint rate for Chinese characters alone measured only 0.09 percent. It is understood that this system will soon be on the market.

Nuclear Reactor Core Fuel Management Software Package Developed

94P60091B Beijing ZHONGGUO KEXUE BAO [CHINESE SCIENCE NEWS] in Chinese 20 Dec 93 p 2

[Article by Zhai Peitian [5049 1014 1131]: "Nuclear Power Software Porting, Development Successful"]

[Summary] The Nuclear Power Institute of China's project involving porting and development of a nuclear power plant reactor core fuel management software package has been successfully completed. This software package, which will be used at domestic nuclear plants for fuel management calculations, is based on imported software that cost the nation 3.48 million francs and was developed by a 21-person institute group led by computer software expert Li Datu [2621 1129 0956]. The package includes two program libraries and seven applications software programs. The project involved making the imported software, written in the Cray computer program language, operate on the VAX machines available here in China, since the Cray and VAX computer program languages are not completely compatible.

Chen Zhaoxiong Transfers IPR 10-Year Use for US$24.44 Million

94P60080A Beijing ZHONGGUO KEXUE BAO [CHINESE SCIENCE NEWS] in Chinese 15 Nov 93 p 1

[Article by Fan Shihong [5400 4355 1347] and Wang Yafen [3769 0068 5358]: "Chen Zhaoxiong's Machine Translation Technology Sets Domestic Intellectual Property Rights Transfer Record: 10-Year Use Will Realize US$24.44 Million"]

[Summary] Dr. Chen Zhaoxiong, the 31-year-old director of the CAS Machine Translation Center, has set a China intellectual property rights (IPR) transfer record: he has granted 10-year rights to use his Kuai Yitong EC863A English-Chinese pocket electronic translation machine technology for US$24.44 million. This unit, 1,000 of which are now being shipped monthly to the United States, Canada, Europe, and Southeast Asia, accounts for an annual output value of almost HK$600 million. Dr. Chen has transferred the rights to his Hong Kong affiliate, the Quanzhi [2938 2535] Company, which is paying Dr. Chen's center US$740,000 for the first year's rights to use the technology.

Additional Details on USTND Simulation/ Modeling Software

94P60080B Beijing JISUANJI SHIJIE [CHINA COMPUTERWORLD] in Chinese No 45, 24 Nov 93 p 1

[Article by Tan Keyang [6223 0344 2254]: "University of Science and Technology for National Defense (USTND) Unveils Simulation and Modeling System"]

[Editorial Report] Additional details on USTND's high-performance general-purpose computer simulation/ modeling system software not already supplied in an earlier report [JPRS-CST-93-019, 15 Dec 93 pp 12-13] are as follows: This "VAX/VMS-oriented simulation and modeling support system, called YHSIM/VMS," is especially targeted to general-purpose mathematical simulations on a VAX machine, but can also function as a powerful tool for teaching Yinhe Fangzhen-II (the YH-F2 simulation computer) users how to use the YFSIM simulation language.

Ground Broken for Southern Software Industrial Park in Zhuhai

94P60080D Beijing JISUANJI SHIJIE [CHINA COMPUTERWORLD] in Chinese No 46, 1 Dec 93 p 1

[Article by Xu Zhou [1776 3166]: "Ground Broken for Southern Software Industrial Park in Zhuhai"]

[Summary] On 29 November, ground was broken for the Southern Software Industrial Park—a State Eighth FYP Key Project—in Zhuhai. Funding and construction are jointly being assumed by the Ministry of Electronics Industry (MEI) and Zhuhai Municipality. Investment for this new park, which will occupy 320,000 square meters in the northeast section of the city, totals almost 300 million yuan RMB, of which half is allocated in the first phase of the project, scheduled to be completed within 2 years. Application software for the domestic and foreign markets will be the primary product. When first-phase construction is completed, it is expected that 15-20 firms, with 1,500 mid-to-senior-level engineers and managers, will take up residence in the park; annual software sales are projected to be 400 million yuan, with 70 percent of the software products to be exported, realizing annual export revenues of 250 million yuan.

Two Domestically Made Lasers Enter U.S. Market

94P60089A Beijing ZHONGGUO KEXUE BAO [CHINESE SCIENCE NEWS] in Chinese 15 Dec 93 p 1

[Article by Yang Zhaoliang [2799 6856 5328]: "Two Complete Laser Systems Developed: Prototypes Find Favor at U.S. Sales Exhibition"]

[Summary] Fuzhou (ZHONGGUO KEXUE BAO wire report)—Prototypes of two new international state-of-the-art entire laser systems developed by the CAS Fujian Institute of Material Structure—the KF-S001 1.3-micron high power CW laser and the KF-D001 dual-wavelength crystal laser (the latter unique worldwide)—recently entered the U.S. market via international cooperative channels, and have attracted much attention at a U.S. sales exhibition begun on 16 November. These two new laser systems, developed by an institute group led by Research Fellow Shen Hongyuan [3088 7703 0337], have the following specifications as measured by the technical appraisal experts: the high-power laser has an output power exceeding 100 watts and the dual-wavelength laser has an output power exceeding 15 watts for each of the wavelengths, while output power stability for both laser systems is better than 1.5 percent. All technical indicators meet or exceed requirements stipulated in the cooperative-development contract signed with the U.S. firm KAIFA.

Color STN-LCD Developed by CAS Changchun Institute of Physics

94P60081C Beijing ZHONGGUO KEXUE BAO [CHINESE SCIENCE NEWS] in Chinese 1 Dec 93 p 2

[Article by Zhong Chunli [0022 2504 3810]: "CAS Changchun Institute of Physics Develops Supertwist-Nematic Liquid Crystal Color Display"]

[Summary] The supertwist-nematic liquid-crystal display (STN-LCD) and [100 x 100-pixel] liquid-crystal color display developed by the CAS Changchun Institute of Physics recently passed formal appraisal, at which the technical experts judged them to meet early-nineties international standards. The experts strongly urge the authorities to provide financial support for this new technology, so that it can be domestically commercialized as soon as possible, with an eye to entering the international STN-LCD product market.

Qinghua University-Developed EDFA Is State-of-the-Art

94P60089B Beijing KEJI RIBAO [SCIENCE AND TECHNOLOGY DAILY] in Chinese 16 Dec 93 p 1

[Article by Fan Jian [5400 1696]: "Qinghua University Develops Erbium-Doped Fiber Amplifier"]

[Summary] Beijing, 15 Dec—A semiconductor-laser-pumped erbium-doped optical fiber amplifier (EDFA) developed by Qinghua University—the nation's first such independently developed EDFA—was just certified by technical experts as having main performance indicators that match the worldwide state-of-the-art. This new EDFA, cooperatively developed with the CAS Institute of Semiconductors, the State Optoelectronics Fabrication Center, MEI's Institute 46, and MPT's Wuhan Institute of Posts and Telecommunications, is the first domestic EDFA to be pumped by 980-nm- and 1480-nm-wavelength laser diodes. Optical gain at the two wavelengths measured 28 dB and 25 dB, respectively; maximum saturated output power was 6.3 milliwatts at both wavelengths; and frequency bandwidth measured 26 nm and 40 nm, respectively.

Institute 44's CCD R&D Line Operational

94P60081D Beijing ZHONGGUO DIANZI BAO [CHINA ELECTRONICS NEWS] in Chinese 3 Dec 93 p 1

[Article by Chen Youhua [7115 3731 5478]: "Eighth FYP CCD R&D Line at Institute 44 Operational"]

[Summary] The charge-coupled device (CCD) R&D line at MEI's Institute 44 is now operational. This Eighth FYP project, begun in September 1990, has resulted in a line with an annual development capacity of 4-6 types of high-quality CCDs, including 3456-pixel and 4096-pixel linear array CCDs and 640,000-pixel and 1-million-pixel [planar-array] B&W and color CCDs.

4096-Pixel CCPD Linear Array Developed by Institute 44

94P60081A Beijing ZHONGGUO DIANZI BAO [CHINA ELECTRONICS NEWS] in Chinese 22 Nov 93 p 3

[Article by Yu Ruming [0151 3067 2494]: "Linear Array 4096-Pixel CCPD Image Pickup Device"; cf. early brief mention in JPRS-CST-93-019, 15 Dec 93 p 19]

[Summary] The linear array 4096-pixel CCPD [charge-coupled photodiode] image pickup device developed by MEI's Institute 44 recently passed formal appraisal. This device, oriented toward airborne and satellite-borne remote sensing, character recognition, image scanning, fax, and industrial measurement and control systems, has a one-row, two-line (up-down two-row shift register) structure, the shift registers being buried-channel CCDs with 3-μm design rules. The device is made with an isoplanar fabrication technique and incorporates photosensitive-area self-alignment and other advanced technologies. Device length is 37.86 mm, conversion efficiency is 99.995 percent, dynamic range is 600:1, dark current density is 10 nA/cm^2, and sensitivity is 1 LX. This is the highest-resolution domestically made linear array CCD to date.

New Radar Automatic Testing System Developed

94P60081B Beijing ZHONGGUO KEXUE BAO [CHINESE SCIENCE NEWS] in Chinese 24 Nov 93 p 2

[Article by Chang Yuli [1603 3768 4409]: "New Radar Automatic Testing System"]

[Summary] Harbin Institute of Technology's Space Institute and the China Aerospace Corporation's Institute 35 have jointly developed the nation's first new radar automatic testing system. This VXI-bus-based system can automatically test 100 parameters of a flight-path radar within 20 minutes.

New Model AlGaAs/GaAs Punch-Through-Type Phototransistor

40100026A Beijing GAO JISHU TONGXUN [HIGH TECHNOLOGY LETTERS] in Chinese Vol 3 No 10, Oct 93 pp 17-19

[English abstract of article by Han Dejun, Li Guohui, et al. of the Institute of Low Energy Nuclear Physics, Beijing Normal University, Beijing 100875, and Zhou Junming and Huang Yi of the Institute of Physics, CAS, Beijing 100080; supported by grant from 863 Plan; MS received 17 Jul 93, revised 2 Sep 93]

[Text] Very-high-sensitivity AlGaAs/GaAs punch-through-type heterojunction phototransistors (PTPT) are studied. They are promising as photodetectors for optical communication systems. The punch-through-type HPT-PTPT (i.e., HPT is designed to operate in such a case that the base region is depleted and punch-through between the emitter and the collector occurs) may perform a high Early-effect enhanced gain. The AlGaAs/GaAs PTPT with a novel guard ring emitter structure is designed and fabricated. The novel guard emitter structure reported here may decrease the capacitance of E-B junction and surface recombination. It has the advantage of increasing the device speed and gain and decreasing noise of device under low incident power condition. Sensitivity of 5500 (μA/μW), current gain of 11,000 and optical gain of 7700 are obtained for an input photo power of 0.4 μW. These values are to the authors' knowledge the highest to date reported for any optical detector. The sensitivity of the PTPT may increase further with decrease of the incident power.

Hybrid Optoelectronic Implementation of Serial Multi-Bit Full Adder

94P60086A Shanghai GUANGXUE XUEBAO [ACTA OPTICA SINICA] in Chinese Vol 13 No 11, Nov 93 pp 1017-1020

[Article by Wang Ruibo [3769 3843 3134], Li Chunfei [2621 3196 7378], and Zhang Lei [1728 7191] of the Dept. of Applied Physics, Harbin Institute of Technology, Harbin 150006: "Hybrid Optoelectronic Implementation of Serial Multi-Bit Full Adder"; MS received 2 Jul 92, revised 16 Nov 92]

[Abstract] An optical binary adder is a critical component in the development of an all-optical digital computer. In the paper, a design for a single-gate serial multi-bit full adder using an optically bistable switch is presented. The operational principle is demonstrated with a ZnS nonlinear interference filter (NLIF) having a center wavelength of 513.7 nm, a minimum open threshold of 11 mW, and a maximum peak transmissivity of 62.4 percent. Experimental results of four-bit addition are reported.

Figures 1-4 (not reproduced) show a schematic of a full adder constructed from two half adders and an OR gate, input-output characteristics required for full-addition operations, a schematic of a single-gate full adder with on-axis and off-axis incidence, and a schematic of a serial full adder, respectively. Figures 5 and 6, reproduced below, show a schematic for a serial full adder using a spatial time-delay cavity and a schematic of the experimental set-up, respectively; in these figures, A_i and B_i are the two input signals, C_{i-1} is the least-significant-bit carry signal, S_i is the sum signal, QWP_1 and QWP_2 are quarter-wave plates, BOS is the bistable optical switch, PBS is a polarizing beam splitter, PD is a photodetector, and TD is a trigger-delay signal generator. Figure 7 (not reproduced) depicts the experimental results: oscilloscope traces for the rising edges of typical transmission and reflection curves and an example of four-bit addition. There are no tables.

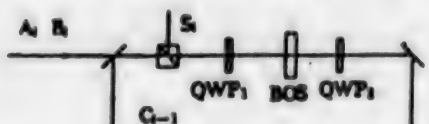

Figure 5. Serial Full-Adder Using Spatial Time-Delay Cavity

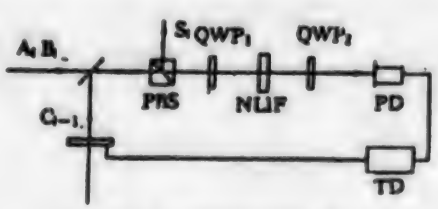

Figure 6. Experimental Set-Up

References

1. Li Chunfei et al., "Optical Full Adder Composed of Two Bistable Devices" [in Chinese], ZHONGGUO JIGUANG [CHINESE JOURNAL OF LASERS], 1989, 16(6): 354-355.

2. Wang Ruibo, Zha Zizhong, Zhang Lei, et al., "All-Optical Full Adder Based on Zinc-Sulphide Optical Bistable Device," 1989 Topical Meeting on Optical Computing, published in 1989, Technical Digest Series: Optical Computing (Optical Society of America), Washington, D.C., 1989: 385-388.

3. F. A. P. Tooley, N. C. Craft, S. D. Smith, et al., "Experimental Realization of an All-Optical Full-Adder Circuit," OPT. COMMUN., 1987, 63(6): 365-370.

4. M. J. Murdocca, A. Huang, J. Jahns, et al., "Optical Design of Programmable Logic Arrays," APPL. OPT., 1988, 27(9): 1651-1660.

Sino-U.S. Joint Venture 'Green' Electronics Plant To Be Built

94P60077A Beijing RENMIN RIBAO OVERSEAS EDITION in Chinese 20 Dec 93 p 2

[Article by Bian Wen [6708 2429]: "China, U.S. To Jointly Build 'Green' Electronics Plant"]

[Text] China's first "green" electronics plant with an air conditioning and purification system cooled without freon is to be built in Dongwan City, Guangdong Province. Construction for this Sino-U.S. joint venture, called Dongwan-Du Pont Electronic Materials Ltd., will begin in 1994, with operation to begin in 1995. According to the bilateral agreement, Dongwan Southern Electronics Ltd. and Du Pont China Group Ltd. will jointly invest US$13 million in the new enterprise, including new microcircuit materials fabrication equipment of the type now used in Du Pont's British, U.S., and Japanese plants. By 1995, the joint venture will start manufacturing thick-film circuits and circuit materials and other electronic devices used in automotive and electronic systems, computers, and similar high-tech products. Half of the output is targeted for the international market and half for the domestic market.

Improved AlGaAs/GaAs Solar Cell Unveiled

94P60082B Beijing ZHONGGUO KEXUE BAO [CHINESE SCIENCE NEWS] in Chinese 24 Nov 93 p 2

[Article by Liu Li [0491 0500]: "Aluminum Gallium Arsenide/Gallium Arsenide Solar Cell Unveiled"]

[Summary] The multiwafer extrusion-boat liquid-phase epitaxy (LPE) AlGaAs/GaAs heterojunction solar cell developed by the CAS Institute of Semiconductors was recently formally certified. Up to 20 epitaxial wafers can be grown per cycle, compared to one wafer per cycle with traditional LPE [graphite-boat] techniques. As measured in vacuum, full-surface conversion efficiency for the two best samples is 18.78 percent and 17.33 percent. The technique is targeted toward solar cells, especially for space vehicle power sources, but is applicable to fabrication of light-emitting devices and other optoelectronic devices as well.

Amorphous Silicon Image Sensor Linear Arrays Developed by CAS Institute of Semiconductors

94P60082A Beijing ZHONGGUO KEXUE BAO [CHINESE SCIENCE NEWS] in Chinese 22 Nov 93 p 2

[Article by Liu Li [0491 0500]: "Amorphous Silicon Image Sensor Linear Arrays Developed by CAS Institute of Semiconductors"]

[Summary] Three amorphous silicon hydride (a—Si:H) image sensor linear arrays developed by the CAS Institute of Semiconductors recently passed expert appraisal. These devices have a number of critical applications in areas such as fax machines, computer document readers and scanners, planar image pickup devices, optical position-sensing detector arrays, high-speed spatial modulators, and X-ray detectors. Fabricated with a plasma enhanced chemical vapor deposition (PECVD) technique, these 40-mm-long 320-element, 25-element, and 16-element a—Si:H arrays exhibit the following main performance indicators: dark current is 1×10^{-12} A, photocurrent-to-dark current ratio is 10^5, and photosensitivity is 0.35 μA/μW (at 600 nm). This device thus has state-of-the-art performance, and can replace imported products.

MBE Growth of GaAs Buffer at Low Temperature

40100029A Beijing BANDAOTI XUEBAO [CHINESE JOURNAL OF SEMICONDUCTORS] in Chinese Vol 14 No 12, Dec 93 pp 768-770

[English abstract of article by Liang Jiben, Kong Meiyang, et al. of the Institute of Semiconductors, CAS, Semiconductor Material Science Laboratory, Beijing 100083; MS received 15 Jul 92, revised 15 Oct 92]

[Text] Low-temperature (LT) growth of GaAs as a buffer layer (BL) with resistivity of 10^8 Ω-cm and optically inactive was grown in a home-made MBE system under arsenic-stable growth conditions at substrate temperatures ranging from 200°C to 300°C and at growth rate of 1 μm/h.

The reflected high-energy electron diffraction pattern was monitored during growth. Although LT-GaAs layer significantly reduces sidegating, it can adversely affect the material quality due to the diffusion of defects from LT-GaAs into the active layer.

A medium layer is inserted between the active layer and LT-GaAs layer. GaAs-AlGaAs superlattice is suggested to prevent the defect diffusion. A relatively small photoluminescence linewidth of 9 meV and high Hall mobility of 10^5 $cm^2/V\text{-}s$ at 77K indicate the high-quality material similar to that of sample without the LTBL.

Formation of Light-Emitting Porous Si Patterns by Preimplantation

40100029B Beijing BANDAOTI XUEBAO [CHINESE JOURNAL OF SEMICONDUCTORS] in Chinese Vol 14 No 12, Dec 93 pp 771-773

[English abstract of article by Yang Haiqiang, Bao Ximao, et al. of the Department of Physics, Nanjing University and Laboratory of Solid State Microstructures, Nanjing 210008; MS received 17 Apr 93, revised 13 Jul 93]

[Text] A new method of fabrication of light-emitting porous Si pattern is reported. Si samples are area-selectively amorphized by self-implantation through an Al mask. After anodization, the light-emitting pattern is obtained. The crystal area emits light, while amorphized region does not. The influence of the ion implantation on formation of porous Si and luminescence is discussed.

Forward Injected Current Detection of Magnetic Resonance in a-Si:H Solar Cell

40100029C Beijing BANDAOTI XUEBAO [CHINESE JOURNAL OF SEMICONDUCTORS] in Chinese Vol 14 No 12, Dec 93 pp 774-777

[English abstract of article by Fu Jishi, Wu En, and Mao Jinchang of the Dept. of Physics, Beijing University, Beijing 100871, Zhu Meidong of the Dept. of Radioelectronics, Beijing University 100871, and Liao Xianbo of the Institute of Semiconductors, CAS, Beijing 100083, MS received 10 May 93]

[Text] An investigation of spin-dependent recombination process in p^+-i-n^+ a-Si:H solar cell by forward injected current detection of magnetic resonance is reported, for the first time. The effects of injected current, illumination on magnetic-resonance signal intensity detected by injected current are studied. The results show that the sensitivity of injected current detection of magnetic resonance is higher than PDMR [photovoltaic detection of magnetic resonance] and this method is suitable for routine assessment for both amorphous and crystalline photovoltaic junction and barrier devices.

Large-Area YBCO Superconducting Thin Film Certified

94P60085B Beijing ZHONGGUO KEXUE BAO [CHINESE SCIENCE NEWS] in Chinese 3 Dec 93 p 1

[Article by Xu Changchun [6079 7022 2504]: "Large-Area Yttrium-Barium-Copper-Oxide Superconducting Thin Film Passes Appraisal"]

[Summary] The microwave devices/circuits-oriented large-area YBCO superconducting thin film developed by Yang Bingchuan's research group at the Beijing General Institute of Nonferrous Metals' Superconducting Materials Research Center recently passed formal appraisal. This thin film, fabricated via the research group's own (and China's first) large-area magnetron sputtering apparatus, can be made as large as 40 mm x 50 mm in one pass. Resonators, filters, superconducting antennas, and other devices fabricated from this thin film have exhibited key performance indicators that meet or approach the worldwide state-of-the-art.

High-Tc Superconducting Bandpass Filter Developed

94P60085A Beijing DIANZI KEXUE XUEKAN [JOURNAL OF ELECTRONICS] in Chinese Vol 15 No 6, Nov 93 pp 663-665

[Article by Cao Xiaoneng [2580 2400 5174], Yang Caibing [2799 1752 3521], et al. of the Institute of Electronics, CAS, Beijing 100080 and Li Hongcheng [2621 1347 2052] and Wang Ruilan [3769 3843 5695] of the Institute of Physics, CAS, Beijing 100080: "High-Temperature Superconducting Bandpass Filter," supported by grant from State Superconductivity R&D Center; MS received 7 Jul 93, revised 9 Aug 93]

[Abstract] A four-pole, parallel-coupled resonant microstrip bandpass filter has been developed via dc magnetron sputtering in-situ deposition of a $GdBa_2Cu_3O_7$ high-Tc superconducting thin film on a (100) $LaAlO_3$ substrate. At 77K, zero-resistance transition temperature of the thin film is 90-92K, critical current density exceeds 10^6 A/cm^2, and film thickness is about 3,000 Angstroms. The bandpass filter was fabricated with a wet chemical etching technique and photolithography with a positive 212 photoresist. At 77K, filter specifications are as follows: frequency range is 7.5-10.5 GHz, center frequency is 8.96 GHz, in-band insertion loss is 0.54 dB, out-band suppression exceeds 45 dB, bandwidth is 500 MHz, and connector type is SMA coaxial. This device is being incorporated into the X-band high-Tc superconducting/semiconductor hybrid integrated receiver front-end circuit now under development by the authors.

Figure 1, reproduced below, is a schematic of the bandpass filter, while Figure 2 (not reproduced) shows a graph of the filter characteristics. There are no tables.

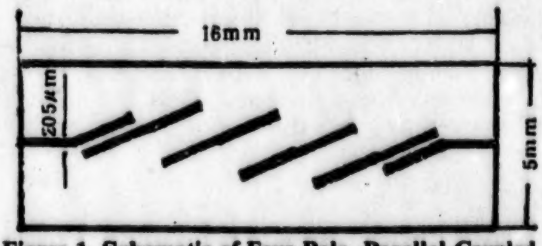

Figure 1. Schematic of Four-Pole, Parallel-Coupled Resonant Microstrip Filter

References

1. D. E. Oates et al., IEEE TRANS. ON MTT, MTT-39 (1991) 9, 1522-1529.
2. S. B. Cohn, IRE TRANS. ON MTT, MTT-6 (1958) 4, 223-231.
3. E. G. Cristal, IEEE TRANS. ON MTT, MTT-19 (1971) 5, 486-490.
4. A. Riddle, "High-Performance Parallel-Coupled Microstrip Filters," IEEE Int. Microwave Symp. Digest, Milpitas [CA], (1988), 427-430.
5. Zhou Wenbiao, "Handbook of Microwave Integrated Circuit CAD" [in Chinese], People's Posts and Telecommunications Publ. House, Beijing, 1988, pp 974-978.
6. L. A. Trinogga et al., "Practical Microstrip Circuit Design," Ellis Harwood, 187-197.
7. D. B. Rensch et al., IEEE TRANS. ON MAG., Mag-27 (1991) 2, 2533-2556.
8. Yi Huairen, Li Hongcheng, et al., BANDAOTI XUEBAO [CHINESE JOURNAL OF SEMICONDUCTORS], 12 (1991) 8, 502-508 [English abstract in JPRS-CST-91-018, 12 Sep 91 p 32].
9. Li Shuqin et al., "Technique for Forming Oxide Superconducting Thin Films" [in Chinese], DIWEN YU CHAODAO [CRYOGENICS AND SUPERCONDUCTIVITY], 18 (1990) 1, 45-49.

Latest Reports on Fiber Optic Communications

New Cable Spans Shandong Peninsula

94P60084A Beijing ZHONGGUO DIANZI BAO [CHINA ELECTRONICS NEWS] in Chinese 22 Nov 93 p 3

[Article by Wang Cuiwen [3769 5050 2429]: "Communications Fiber Optic Cable Spans Shandong Peninsula"]

[Summary] Construction of the Weifang-to-Yantai fiber optic cable is just about underway. This 308-km-long, 33-million-yuan project in its initial phase will have three DS4 [140 Mbps] systems and one inter-district system, totaling 7,680 circuits.

Course of Domestic Development

94P60084B Beijing ZHONGGUO DIANZI BAO [CHINA ELECTRONICS NEWS] in Chinese 29 Nov 93 p 3

[Article by Qian Zongjue [6929 1350 3778], chief engineer, MPT Science and Technology Department: "Development Course of Nation's Fiber Optic Communications"]

[Excerpt] [Passage omitted] The 8B1H-encoding-type DS5 (565 Mbps, 7,680-circuit) trunk line fiber optic cable system connecting Shanghai and Wuxi is already operational, and is to be extended to Nanjing, with further development.

Among the critical issues in determining the development course of the nation's fiber optic communications technology in the Eighth FYP, one of the most important is whether to include Synchronous Digital Hierarchy (SDH) tasks as Key Eighth FYP Projects. After sufficient investigation, it has been decided that the following will be Key Eighth FYP Projects: SDH's STM-1 (155 Mbps) and STM-4 (622 Mbps), as well as digital cross-connect (DXC) equipment and 565 Mbps [DS5] fiber optic cable communications system technologies, all of which have been basically studied and which are to be made more utilitarian. MPT's Institute 5 and the Wuhan Institute of Posts and Telecommunications have been the leading organizations in optical SDH research. Simultaneously, the State 863 Plan's Optoelectronics Topical Area and a newly formed "Communications High Technology" Expert Topical Area have exerted great effort toward development of STM-16 (2.5 gigabit/s) optical communications systems.

It is hoped that the nation's fiber optic communications technology will achieve new breakthroughs in 1995.

Applications, Development Directions

94P60084C Beijing ZHONGGUO DIANZI BAO [CHINA ELECTRONICS NEWS] in Chinese 6 Dec 93 p 3

[Article by Qian Zongjue [6929 1350 3778], chief engineer, MPT Science and Technology department: "Applications, Development Directions for Domestic Fiber Optic Communications"]

[Summary] The nation's fiber optic communications trunk line backbone is taking shape in the current (Eighth) FYP, with Beijing as the hub, pointing toward the East, West, South, North, and Central parts of China. The construction plan is as follows:

Beijing-to-Northeast: Two fiber optic cable trunk lines—Beijing-Tianjin-Shenyang-Changchun-Harbin and Beijing-Chengde-Fuxin-Baicheng-Qiqihar—and four branch lines have formed a mesh network covering the Beijing-Tianjin-Tangshan economically developed region and the three Northeast provinces, as well as the eastern part of Inner Mongolia.

Beijing-to-Southeast and Seacoast: The Beijing-Tianjin-Nanjing and Nanjing-Shanghai fiber optic cable trunk lines are being linked to the Shanghai-Fuzhou-Guangzhou fiber optic cable trunk line forming a Southern Seacoast Economic Development Area information network.

Beijing-to-Central China and the South: Two Beijing-Wuhan-Guangzhou fiber optic cable trunk lines—one overhead, one buried—are being built and will be interconnected with the Southern Seacoast fiber optic cable trunk line and the Northwest fiber optic cable trunk line into a backbone.

Beijing-to-Northwest and Southwest: Three fiber optic cable trunk lines—Beijing-Hohhot-Yinchuan-Lanzhou, Beijing-Taiyuan-Xian, and Xian-Lanzhou—are forming a ring network extending westward to Urumqi and eventually further west to Yining. The Chengdu-Chongqing-Guiyang-Changsha-Nanchang-Fuzhou (Hangzhou) fiber optic cable trunk line and the Chengdu-Kunming, Kunming-Nanning, Nanning-Guangzhou, and Guangzhou-Haikou fiber optic cable trunk lines (which form a chain that has linked up the Southwest in a large ring) together have formed a mesh fiber optic cable trunk line network covering the Southwest.

Fiber Optic Cables Spanning the South-Central and Eastern Areas: Wuhan-Chongqing, Xuzhou-Zhengzhou, Zhengzhou-Xian, Xian-Chengdu and other fiber optic cable trunk lines are being built.

All of these fiber optic cable trunk lines, totaling 32,000 km in length, will be completed by the end of 1995. The aforementioned 22 fiber optic cable trunk lines will be interconnected with 20 interprovincial microwave trunk

lines and 19 satellite earth stations to form a three-dimensional nationwide digital communications trunk line network.

Domestic research institutes and commercial firms have begun to explore future-oriented technologies. In the area of trunk line fiber optic cable networks, new development directions include conventional intensity-modulation direct detection (IMDD) technology, SDH and DXC technologies, and further efforts to utilitarianize erbium-doped fiber amplifier (EDFA) and dense wavelength-division multiplexing (DWDM) technologies. In the area of local subscriber loops (fiber optic cable networks), new development directions include fiber-in-the-loop (FITL), cable TV (CATV), and asynchronous transfer mode (ATM) technologies. In the third and final area of undersea fiber optic cable networks, new development directions include interconnection with the Southern Seacoast fiber optic cable trunk line network and global networks, as well as new optoelectronic integrated circuit technology, optical amplifiers, WDM technology, and optical soliton communications technology.

New Products From Wuhan Institute

94P60084D Beijing ZHONGGUO DIANZI BAO [CHINA ELECTRONICS NEWS] in Chinese 12 Dec 93 p 2

[Article by Sun Yushan [1327 3768 1472]: "Several New Optical Fiber, Fiber Optic Cable Products From Wuhan Hit Market"]

[Summary] Ten new fiber optic products—four varieties of fiber and six varieties of fiber optic cable—recently developed by the Wuhan Institute of Posts and Telecommunications Science are now on the market.

The new optical fiber varieties are: 1) dispersion-shifted fiber, with a zero-dispersion wavelength near 1.3 μm, 2) quartz multimode fiber, 3) single-mode polarization-maintaining fiber, and 4) plastic fiber.

The new fiber optic cable varieties are: 1) overhead duct cable, 2) buried cable, 3) underwater cable, 4) nonmetallic cable, 5) splicing-box cable, and 6) terminal-box cable.

Beijing-Wuhan-Guangzhou Overhead Cable

94P60092A Beijing ZHONGGUO DIANZI BAO [CHINA ELECTRONICS NEWS] in Chinese 13 Dec 93 p 3

[Article by Zhu Fuchang [2612 4395 2490]: "Beijing-Wuhan-Guangzhou Fiber Optic Cable Project Uses Domestically Made Equipment Throughout"]

[Summary] The five-province, 3074-km-long Beijing-Wuhan-Guangzhou fiber optic cable communications project, which uses 12-core overhead cable and 1B1H encoding, is the world's longest overhead fiber optic cable. Throughout, the cable incorporates domestically made equipment jointly developed and manufactured by the State Fiber Optic Communications Technology Engineering Research Center and Sichuan's Meishan Communications Equipment Plant. Circuit transmission capacity is 1920 + 1200 circuits, which is 1200 circuits (for interdistrict telephone service) more than possible with other encoding formats.

Beijing-Jinan-Nanjing Cable

94P60092B Beijing ZHONGGUO DIANZI BAO [CHINA ELECTRONICS NEWS] in Chinese 13 Dec 93 p 3

[Article by Jiang You [3068 1429]: "Beijing-Jinan-Nanjing Fiber Optic Cable Communications Trunk Line Operational"]

[Summary] The nation's first high-capacity, long-distance communications trunk line using domestically made optical communications equipment throughout—the Beijing-Jinan-Nanjing fiber optic cable trunk line—became formally operational a few days ago. This 1444-km-long, 230-million-yuan trunk line connects Beijing with Tianjin, Cangzhou, Jinan, Xuzhou, Bengbu, Hefei, and Nanjing, and provides 20,000 interprovincial trunk line long-distance circuits and 25,000 intraprovincial, inter-county circuits. The entire project uses 24-core cable with DS4 [140 Mbps] transmission equipment. So far, almost 6,000 service lines have been connected.

END OF FICHE

DATE FILMED

10 MAR 1994